Clim. Past, 17, 1955–1972, 2021
https://doi.org/10.5194/cp-17-1955-2021

Climate of the Past
Open Access
EGU

Palaeo-environmental evolution of Central Asia during the Cenozoic: new insights from the continental sedimentary archive of the Valley of Lakes (Mongolia)

Andre Baldermann[1], Oliver Wasser[1], Elshan Abdullayev[2,3], Stefano Bernasconi[4], Stefan Löhr[5], Klaus Wemmer[6], Werner E. Piller[7], Maxim Rudmin[8], and Sylvain Richoz[9]

[1]Institute of Applied Geosciences, Graz University of Technology, NAWI Graz Geocenter, Graz, Austria
[2]Department of Life Sciences, Khazar University, Baku, Azerbaijan
[3]Department of Geoscience, French-Azerbaijani University (UFAZ), Baku, Azerbaijan
[4]Geological Institute, ETH Zurich, Zurich, Switzerland
[5]Department of Earth and Environmental Sciences, Macquarie University, Sydney, Australia
[6]Geoscience Centre (GZG), University of Göttingen, Göttingen, Germany
[7]Institute of Earth Sciences, University of Graz, NAWI Graz Geocenter, Graz, Austria
[8]Division of Geology, Tomsk Polytechnic University, Tomsk, Russia
[9]Department of Geology, University of Lund, Lund, Sweden

Correspondence: Andre Baldermann (baldermann@tugraz.at)

Received: 23 March 2021 – Discussion started: 25 March 2021
Revised: 19 July 2021 – Accepted: 30 August 2021 – Published: 29 September 2021

Abstract. The Valley of Lakes basin (Mongolia) contains a unique continental sedimentary archive, suitable for constraining the influence of tectonics and climate change on the aridification of Central Asia in the Cenozoic. We identify the sedimentary provenance, the (post)depositional environment and the palaeo-climate based on sedimentological, petrographical, mineralogical, and (isotope) geochemical signatures recorded in authigenic and detrital silicates as well as soil carbonates in a sedimentary succession spanning from ∼ 34 to 21 Ma. The depositional setting was characterized by an ephemeral braided river system draining prograding alluvial fans, with episodes of lake, playa or open-steppe sedimentation. Metamorphics from the northern adjacent Neoarchean to late Proterozoic hinterlands provided a continuous influx of silicate detritus to the basin, as indicated by K–Ar ages of detrital muscovite (∼ 798–728 Ma) and discrimination function analysis. The authigenic clay fraction is dominated by illite–smectite and "hairy" illite (K–Ar ages of ∼ 34–25 Ma), which formed during coupled petrogenesis and precipitation from hydrothermal fluids originating from major basalt flow events (∼ 32–29 and ∼ 29–25 Ma). Changes in hydroclimate are recorded in $\delta^{18}O$ and $\delta^{13}C$ profiles of soil carbonates and in silicate mineral weathering patterns, indicating that comparatively humid to semi-arid conditions prevailed in the late(st) Eocene, changing into arid conditions in the Oligocene and back to humid to semi-arid conditions in the early Miocene. Aridification steps are indicated at ∼ 34–33, ∼ 31, ∼ 28 and ∼ 23 Ma and coincide with some episodes of high-latitude ice-sheet expansion inferred from marine deep-sea sedimentary records. This suggests that long-term variations in the ocean–atmosphere circulation patterns due to pCO_2 fall, reconfiguration of ocean gateways and ice-sheet expansion in Antarctica could have impacted the hydroclimate and weathering regime in the basin. We conclude that the aridification in Central Asia was triggered by reduced moisture influx by westerly winds driven by Cenozoic climate forcing and the exhumation of the Tian Shan and Altai Mountains and modulated by global climate events.

1 Introduction

The Cenozoic era (66 Ma to the present day) saw several dramatic changes in the marine and continental ecosystems (e.g. the evolution of large plankton feeders such as baleen whales, a shift towards cold-water high-nutrient plankton assemblages at high latitude and the expansion of terrestrial mammals), major tectonic events (e.g. opening of Southern Hemisphere oceanic gateways, shift to the four-layer structure of the modern ocean, collision of the African–Arabian–Eurasian plates, and uplift of the Alpine and Himalayan mountain belt) and global climate forcing (e.g. change from greenhouse to icehouse conditions) (Cerling, 1993; Houben et al., 2013; Norris et al., 2013; Cermeño et al., 2015; Mutz et al., 2018; Komar and Zeebe, 2021). The acceleration of Cenozoic climate cooling started after the early Eocene climatic optimum (EECO; ∼ 52–50 Ma), with temperatures ∼ 10–12 °C warmer than the modern deep ocean, followed by the appearance and expansion of the Antarctic ice sheets after the Eocene–Oligocene transition (EOT; ∼ 34 Ma) and ultimately culminating in the extensive Northern Hemisphere glaciation of the Pleistocene (∼ 2.6–0.01 Ma; Zachos et al., 2001; Lear et al., 2008; Mudelsee et al., 2014; Abdullayev et al., 2021). This long-term transition in Earth's climate is well documented in marine sedimentary archives, but its impact on the evolution of continental ecosystems remains poorly constrained, mainly because continuous, well-preserved terrestrial records are scarce and the responses to climate change in these settings are highly complex, depending on factors such as latitude, proximity to coast and mountain ranges, position relative to climatic winds, and vegetation (e.g. Caves Rugenstein and Chamberlain, 2018; Baldermann et al., 2020). An exception is the sedimentary archive of the Valley of Lakes (Mongolia), which hosts a ∼ 34–21 Ma record of continental sedimentation in Central Asia. The biostratigraphy and the correlation between different outcrops in this basin are well established based on mammalian communities and gastropod records (Harzhauser et al., 2017), magnetostratigraphy (Sun and Windley, 2015), and radiometric age dating of different basalt horizons (Daxner-Höck et al., 2017), rendering this locality suitable for constraining the links between tectonism and climate change in Central Asia during the Cenozoic. The Eocene to Miocene period in Central Asia was characterized by accelerated aridification (Dupont-Nivet et al., 2007; Xiao et al., 2010; Bosboom et al., 2014; Li et al., 2016), expressed as a substantially expanded Gobi Desert relative to today (Guo et al., 2008; Lu et al., 2019) and a sudden turnover in the mammal record (Harzhauser et al., 2016; Barbolini et al., 2020). Several, partially opposing hypotheses have been proposed to explain the aridification of Central Asia, including a combination of orbitally driven climate forcing, the stepwise retreat of the proto-Paratethys Sea and uplift of the Tibetan Plateau (Pälike et al., 2006; Zhang et al., 2013; H. Li et al., 2020), or a continuous decrease in moisture transport by the westerlies due to exhumation of the Tian Shan and Altai Mountains (Caves et al., 2014, 2015; Caves Rugenstein and Chamberlain, 2018). However, the evolution of Central Asia's hydroclimate in the Cenozoic was not a period of continuous aridification; indeed, the climatic conditions, in particular in the Oligocene, were highly complex and characterized by numerous glacial–interglacial cycles (Xiao et al., 2010). Recently, Richoz et al. (2017) identified two aridification pulses in Central Asia, in the early and late Oligocene, which they assigned to global climatic events. To date, a correlation of the global marine record with the terrestrial record of Mongolia has barely been developed (Harzhauser et al., 2016, 2017; Richoz et al., 2017), which limits our understanding of the relative influences of climate change and regional tectonics on the evolution of hydroclimate and weathering conditions in Central Asia in the Cenozoic.

In this contribution, we greatly extend the existing mineralogical and (isotope) geochemical dataset previously reported in Richoz et al. (2017) for the Eocene–Miocene sediments from the Valley of Lakes (Mongolia): K–Ar ages and polytype analysis of detrital and authigenic illitic phases coupled with discrimination function analysis and sedimentological–petrographical–geochemical inspection are used to constrain provenance, palaeo-environmental conditions and post-depositional alteration history of this sedimentary succession. Systematic, coherent changes in the weathering patterns of silicate detritus and pristine $\delta^{18}O$ and $\delta^{13}C$ signatures recorded in paleosols' carbonates allow us to revise and refine the evolution of hydroclimate and weathering conditions in Central Asia in the Cenozoic.

2 Geological framework

The Valley of Lakes is an ESE–WNW-striking sedimentary basin with ∼ 500 km extension in its largest dimension. It is located in Central Mongolia and bordered by the Khangai Mountains in the north and the Gobi Altai Mountains in the south (Fig. 1a). The geological super-units in the north of Mongolia contain Neoarchean, Proterozoic and Palaeozoic rocks of the Caledonian orogen as well as late Neoproterozoic to Ordovician (Tuva-Mongol) magmatic arc and related back- and fore-arc intrusions, accretionary wedge sequences, and ophiolites (Porter, 2016). The geological super-units in the south are characterized mainly by a Palaeozoic orogen, especially the Kazakh-Mongol magmatic arc, which forms the border between Mongolia and China. These units include mainly Devonian to Carboniferous island arc volcanic rocks, Ordovician to Silurian volcanics, Ordovician to Carboniferous metamorphosed sedimentary sequences and Permo-Carboniferous granitoids (Porter, 2016).

Regarding the regional lithostratigraphic context, the northern structural units of the Valley of Lakes basin in the Taatsiin Gol area comprise dominantly fault- and thrust-bounded crystalline basement of Neoarchean to Palaeo-

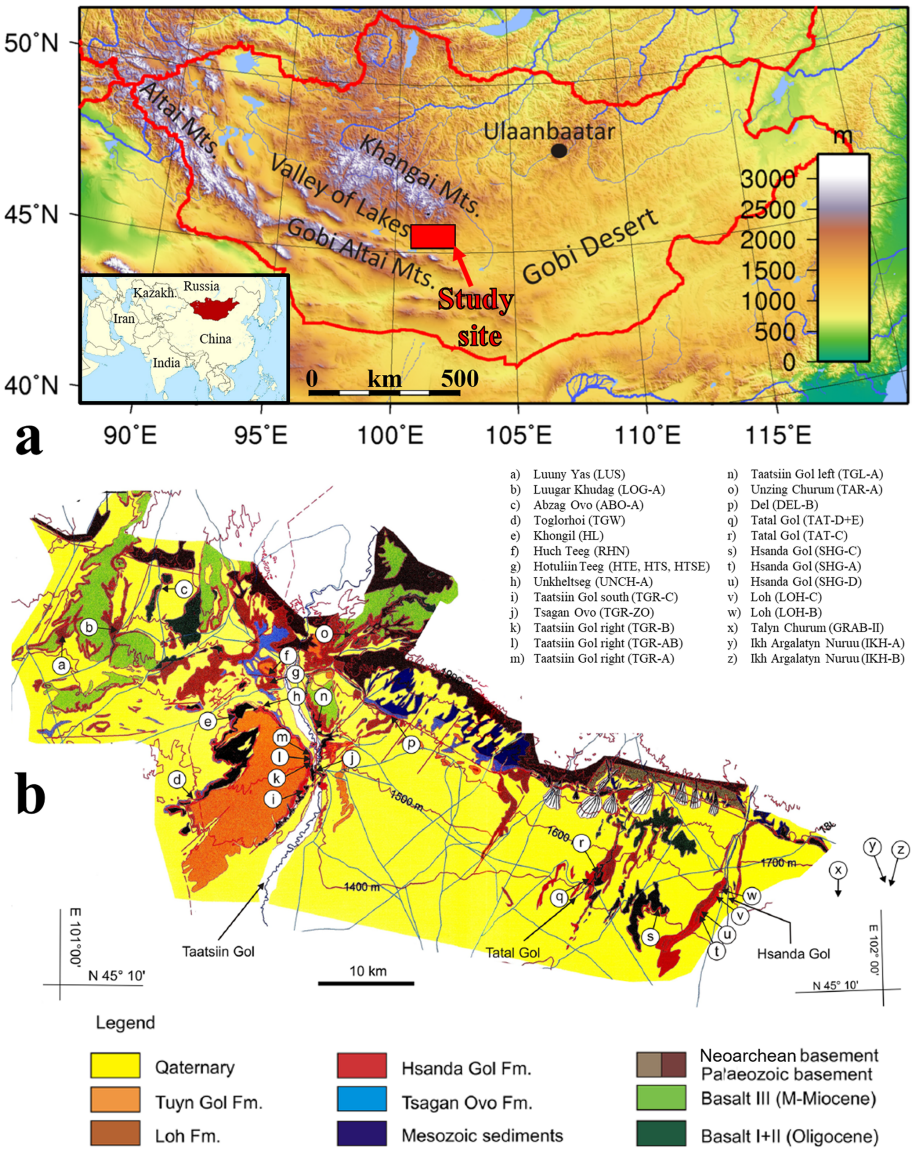

Figure 1. **(a)** Location of the study site in the Taatsiin Gol region, a part of the Valley of Lakes, in Mongolia (Central Asia). The altitude in metres is indicated on the right. **(b)** Geological map of the Taatsiin Gol area within the Valley of Lakes with the sampling sites marked in alphabetical order (modified after Daxner-Höck et al., 2017).

zoic age (Fig. 1b). These include the Baidrag (high-grade gneisses, charnockites and amphibolites, up to 2.65 Ga old) and the Burd Gol zone (metapelites, metapsammites and metacherts, 699 ± 35 Ma) in its southernmost end (Teraoka et al., 1996). Further structural units towards the north are the Bayan Khongor (metamorphosed basic rocks, ophiolites and pelitic schists, 450 Ma), the Dzag (metapelites and metapsammites, 440 ± 22 and 395 ± 20 Ma) and the Khangai zone (unmetamorphosed but tectonically deformed sandstones, mudstones and intercalated olistolith sequences of unspecified Devonian to Carboniferous age) (Teraoka et al., 1996; Höck et al., 1999). All of these zones are intruded by numerous granitoids of variable age (Proterozoic to Cretaceous) and composition (Höck et al., 1999). The major zones located in the south of the Valley of Lakes basin comprise the Baga Bogd, the Ikh Bogd and the Bogd Som, which are petrographically indistinguishable from the time-equivalent metasediments and metavolcanics of the Bayan Khongor zone and of the Permian quartzitic conglomerates from the adjacent Mount Ushgoeg (Höck et al., 1999).

The focus of this study are the fossiliferous siliciclastic sediments of the Taatsiin Gol Basin, which record important information about changes in sediment provenance, weathering paths and conditions, and palaeo-climate in Central Asia during the Eocene to Miocene. The herein investigated sedimentary sections span the Tsagaan Ovoo Forma-

tion (upper Eocene), the Hsanda Gol Formation (Oligocene) and the Loh Formation (lower Miocene). Five sections, namely Taatsiin Gol right (TGR-AB), Taatsiin Gol south (TGR-C), Hsanda Gol (SHG-D), Tatal Gol (TAT-E) and Hotuliin Teeg (HTE), were chosen for this study, due to the well-constrained chronological framework at these localities. Based on previous radiometric and magnetostratigraphic dating of these sections (Höck et al., 1999; Sun and Windley, 2015), Harzhauser et al. (2017) established a precise biozonation of the studied sedimentary succession, which includes, from the bottom to the top, Zone A (early Rupelian: 33.9 to ∼ 31.5 Ma), Zone B (late Rupelian: ∼ 31.5 to ∼ 28.1 Ma), Zone C (early Chattian: ∼ 28.1 to ∼25.6 Ma), Zone C1 (mid-Chattian: ∼ 25.6 to ∼ 24.0 Ma), Zone C1-D (late Chattian ∼ 24.0 to ∼ 23.0 Ma) and Zone D (Aquitanian: ∼ 23.0 to ∼ 21.0 Ma).

These sections form an integrated sedimentary succession with a thickness of ∼ 115 m (Richoz et al., 2017). Two prominent stratigraphic marker beds, the basalt I group (32.4–29.1 Ma) and the basalt II group (28.7–24.9 Ma) crop out at ∼ 40–41 m and ∼ 94–100 m in the sedimentary profile respectively (Daxner-Höck et al., 2017). A younger basalt III group (13.2–12.2 Ma) dates back to the middle Miocene but is not part of the sedimentary succession investigated here. Further details about the local nomenclature, the investigated profiles, profile correlation and lithostratigraphic relationships are provided in Harzhauser et al. (2017), Daxner-Höck et al. (2017) and Richoz et al. (2017). Due to the complex architecture of the Valley of Lakes basin and adjacent areas, a mixed provenance has been proposed for the basin fill; however, detailed knowledge about the palaeo-depositional environment and source area relationships remain poorly constrained (Höck et al., 1999).

3 Materials and methods

3.1 Materials

Representative bulk sediment samples (140 in total) were taken from different outcrops, which cover the entire sedimentary succession of the Valley of Lakes from the upper Eocene to the lower Miocene. The layers sampled vary with respect to parameters such as colour, composition, texture, fossil and carbonate content; however, they do not show optical signs of alteration, such as recent surface weathering. Samples for geochemical, isotopic and mineralogical analysis were crushed in a ball mill for 10 min and micronized using a McCrone mill for 8 min, with ethanol addition. Samples with a high clay mineral content based on an initial mineralogical inspection were selected for further identification of the clay mineral suite, which is defined here as the <2 µm size fraction (Rafiei et al., 2020). As for the clay mineral separation, 5 g of the bulk material was reacted with 5 % HCl for 10 min to remove the carbonates, followed by standard Atterberg sedimentation and subsequent collection and drying of the <2 µm size fraction at 40 °C. Fast acid digestion was used to reduce leaching or dissolution of the clay minerals under acidic conditions (Baldermann et al., 2012). Four samples from the Hsanda Gol Formation with a high amount of illitic phases were used for an illite polytype and K–Ar analysis. To this end, three subfractions (<1, 1–2 and 2–10 µm) were separated by Atterberg sedimentation, which all represent mixtures of authigenic illitic phases and detrital illite/muscovite.

3.2 Analytical methods

The major, minor and trace element composition of a subset of samples (91 in total) was analysed via a Philips PW2404 wavelength dispersive X-ray fluorescence (XRF) spectrometer. Fine powdered samples (0.8 g) were heated to 1050 °C to remove the volatile components (e.g. CO_2, H_2O), following determination of the loss on ignition (LOI) by gravimetric analysis. The residuals were fused at 1200 °C using $LiBO_2$ (4 g) as the fluent agent. The standard glass tablets were analysed together with a set of United States Geological Survey (USGS) standards (analytical error of ±0.5 wt % for the major elements; Richoz et al., 2017).

Sediment origin and variations in the detrital influx among the different provenance areas were depicted using discrimination plots calculated on the basis of major oxide compositions (Roser and Korsch, 1988). The weathering paths and intensities in the source rock areas were assessed through changes in the weathering indices, such as the chemical index of alteration (CIA), the chemical index of weathering (CIW) and the plagioclase index of alteration (PIA), which were calculated based on the major oxide compositions using the following equations (Nesbitt and Young, 1982; Abdullayev et al., 2021):

$$\mathrm{CIA} = (\mathrm{Al_2O_3}/(\mathrm{Al_2O_3} + \mathrm{CaO^*} + \mathrm{Na_2O} + \mathrm{K_2O})) \times 100,$$

$$\mathrm{CIW} = (\mathrm{Al_2O_3}/(\mathrm{Al_2O_3} + \mathrm{CaO^*} + \mathrm{Na_2O}) \times 100,$$

$$\mathrm{PIA} = (\mathrm{Al_2O_3} - \mathrm{K_2O})/(\mathrm{Al_2O_3} + \mathrm{CaO^*} + \mathrm{Na_2O} - \mathrm{K_2O}) \times 100,$$

where CaO^* denotes the fraction of CaO present in the silicate fraction. CaO^* was calculated by subtraction of the total CaO content of the bulk sediments (determined by XRF analyses) from the CaO content associated with carbonate minerals (determined by XRD analyses, see below). The weathering conditions of the source areas were identified further using $Al_2O_3 - CaO^* + Na_2O - K_2O$ (A–CN–K) ternary diagrams (Nesbitt and Young, 1984).

The mineralogical composition of all bulk samples was determined by Rietveld-based analysis of X-ray diffraction (XRD) patterns recorded on a PANalytical X'Pert PRO diffractometer (Co–Kα; 40 kV and 40 mA) equipped with a high-speed Scientific X'Celerator detector. The top loading technique was used for the preparation of randomly oriented samples, which were examined in the range from 4 to 85 2θ with 0.008° 2θ/s step size and 40 s count time. The

PANalytical X'Pert HighScore Plus software and a PDF-4 database were used for mineral quantification (analytical error of <3 wt %; Baldermann et al., 2021a). The separated grain size subfractions were X-rayed under identical operational conditions. The amounts of authigenic (1M and $1M_d$ polytype) and detrital ($2M_1$ polytype) illitic phases were calculated using the following equations (Grathoff and Moore, 1996):

$$\%2M_1 = 2.05 + 360 \times A_{(114)}/A_{(2.6\,\text{Å band})},$$
$$\%1M = 4.98 + 136 \times A_{(-112)}/A_{(2.6\,\text{Å band})},$$
$$\%1M_d = 100 - \%1M \text{ or } 100 - \%2M_1,$$

where A is the area (in cps $\cdot 2\theta$) of the polytype-specific hkl-reflections of illite and of the 2.6 Å band respectively (analytical error of $\sim \pm 5$ %; Baldermann et al., 2017).

Oriented clay films were prepared for the further characterization of the clay mineral fraction (<2 µm) using a Philips PW1830 diffractometer (Cu–Kα; 40 kV and 30 mA) outfitted with a graphite monochromator and a scintillation counter. The clay films were prepared by mixing 50 mg of clay fraction with 5 mL of deionized water, following ultrasonic treatment in a water bath for 10 min to produce a clay in suspension, which was subsequently sucked through a porous ceramic tile of $\sim 4\,cm^2$ size (Baldermann et al., 2014). The clay films were examined in the range from 3 to 30° 2θ with a 0.02° 2θ step size and a 2 s per step count time, each at air-dry states, after solvation with ethylene glycol (EG) and after heat treatment at 550 °C for 1 h. The proportion of illite layers (%Ilt) in mixed-layered illite–smectite (Ilt–Smc) was calculated based on the position of the 002 reflections obtained from XRD patterns of EG-solvated clay films ($d_{\text{EG-002}}$ in Å) according to the following equation (analytical precision of ±5 %; Baldermann et al., 2017):

$$\%\text{Ilt} = 60.8 \times d_{\text{EG-002}} - 504.5.$$

Illite crystallization ages were calculated through coupled illite polytype and K–Ar analysis carried out on the separated grain size subfractions. The K_2O content of these samples was determined in digested aliquots (1M HF and HNO_3 mixture) in duplicate via a BWB-XP flame photometer™ using 1 % CsCl as the ionization buffer and 5 % LiCl as the internal standard. The Ar isotopic composition was analysed in a stainless-steel extraction and purification line connected to a Thermo Scientific Argus VI™ noble gas mass spectrometer operated in static mode at the University of Göttingen (Germany). The radiogenic ^{40}Ar content was measured using the standard isotope dilution method applying a highly enriched ^{38}Ar spike calibrated against the biotite standard HD-B1. K–Ar age calculations were made based on the constants recommended by the International Union of Geological Sciences (IUGS; for details, see Wemmer et al., 2011). The grain size subfractions are free of K-containing mineral phases other than mica/illite group minerals, which would disturb the radiogenic K–Ar ages.

A scanning electron microscopy (SEM) study was carried out to characterize the mineralogy, chemical composition, microfabrics, and alteration patterns of the authigenic and detrital (clay) minerals present in the sediments. Therefore, specimens were prepared on standard SEM stubs, coated with carbon, and analysed using a GEMINI® Zeiss Ultra 55 microscope operated at 5–15 kV of accelerating voltage and equipped with a high-efficiency in-lens secondary electron (SE) detector and an EDAX Si(Li) detector for high-resolution imaging and energy-dispersive X-ray spectrometry (EDX) analysis.

The $\delta^{13}C$ and $\delta^{18}O$ isotopic composition of the carbonate fraction was analysed to constrain the palaeo-climatic trends recorded in the paleosols. In a previous study (Richoz et al., 2017), it was shown that the soil carbonates (calcrete nodules, lenses and crusts) mostly record pristine $\delta^{13}C$ and $\delta^{18}O$ isotopic compositions that are reflective of conditions during their formation and are not influenced by detrital or secondary carbonates, such as calcite spar or dolomite. The samples (139 in total) were reacted with 102 % phosphoric acid at 70 °C in a Kiel II automated reaction system, and the liberated CO_2 gas was analysed with a Thermo Finnigan MAT DELTA mass spectrometer. The measured $\delta^{13}C$ and $\delta^{18}O$ values were corrected against the NBS19 standard and are reported in per mill (‰) relative to the Vienna PeeDee Belemnite (V-PDB) standard (analytical precision of <0.05 ‰ for $\delta^{13}C$ and <0.1 ‰ for $\delta^{18}O$; Richoz et al., 2017).

4 Results

4.1 Sediment petrography

An integrated lithostratigraphic profile of the investigated sedimentary succession (upper Eocene to lower Miocene) from the Taatsiin Gol region, which is a part of the Valley of Lakes, including the biozonation and some field impressions, is presented in Fig. 2.

The sediments from the Tsagaan Ovoo Formation (upper Eocene) are dominantly coarse clastic sand and gravel deposits of white–greyish colour with embedded clay and silt layers of greyish-yellow-green to reddish-brown colour, depending on the Fe content (Richoz et al., 2017). The coarser beds show cross-bedding and are frequently poorly sorted, while the finer layers show trough and planar cross-bedding, lamination, inverse to normal grading, rarely ripples and channel fills, and are better sorted. Roots and plant debris and bioturbation features, such as burrows, indicate local paleosol formation (Richoz et al., 2017).

The overlying Hsanda Gol Formation (Oligocene) has a higher fossil content (mainly the remains of small mammals) and appears as horizontally bedded and poorly sorted clay to silt layers of brick-red to reddish-brown colour with intercalated cross-bedded sandstone beds and minor sand and

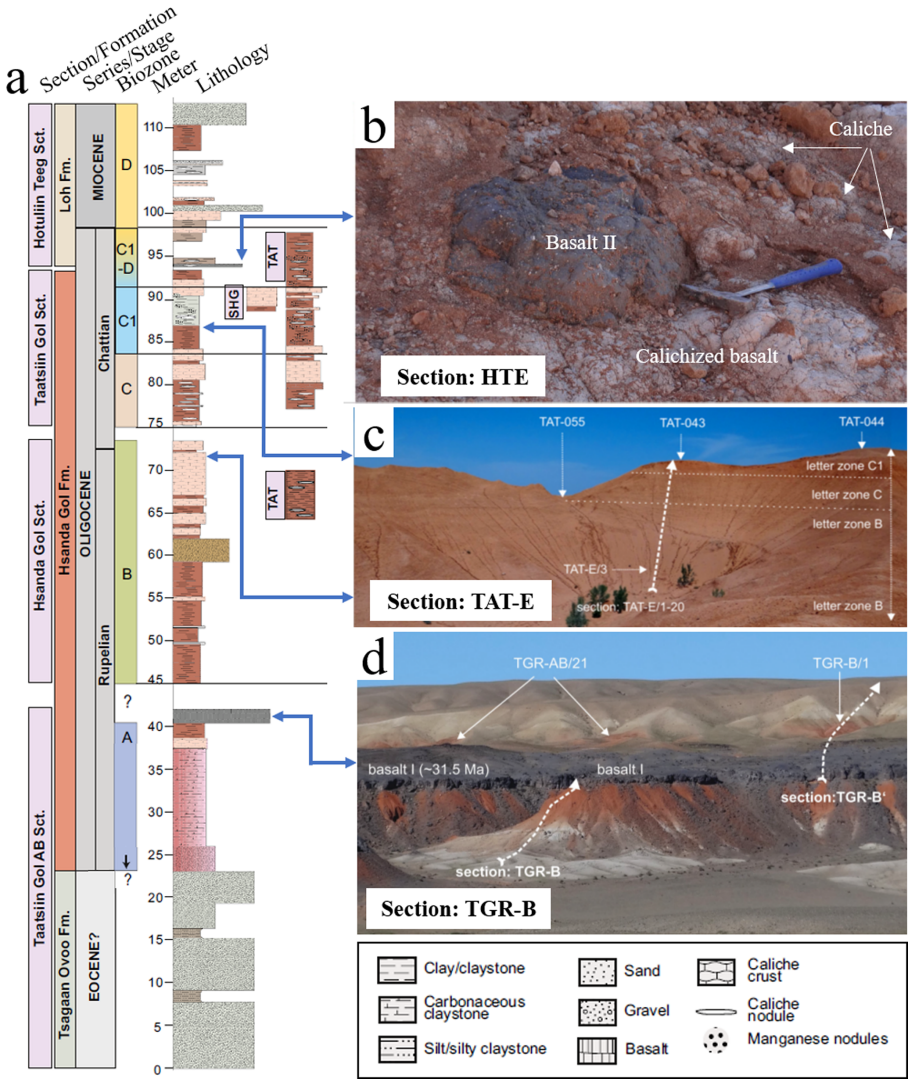

Figure 2. **(a)** Integrated lithostratigraphic profile of the investigated sedimentary succession from the Taatsiin Gol region, Valley of Lakes (modified after Richoz et al., 2017), with biozonation (modified after Harzhauser et al., 2017). **(b–d)** Field impressions of the sections: Hotuliin Teeg (HTE) with the calichized basalt II group, Tatal Gol (TAT-E) sediments and the Taatsiin Gol right (TGR-B) section with the basalt I group (modified after Daxner-Höck et al., 2017).

granule lenses of greyish colour (Fig. 2c). Paleosol formation is documented by abundant crypto- to microcrystalline calcite nodules and calcite crusts of centimetre to decimetre size encapsulating soil and plant materials (Fig. 2b; Richoz et al., 2017). These calcrete layers of greyish-white colour are partially intergrown with Fe- and Mn-(oxy)hydroxides of orange-greyish-black colour. The basalt I and basalt II horizons are exposed at ∼ 40–41 m and at ∼ 94–100 m respectively and interfinger with the sediments from the Hsanda Gol Formation (Fig. 2b, d).

The Loh Formation (lower Miocene) comprises generally poorly sorted and structure-less silty–clayey horizons with embedded pebbles and lenses of greyish-white to reddish-brown colour as well as trough to planar cross-bedded sand and gravel beds that are green, yellow, red or a mixture of the aforementioned colours and are deposited in alternate mode. Sedimentary structures seen in the coarser beds include inverse to normal grading, ripple marks, channel and scour fills, and overbank fines (Richoz et al., 2017). Most horizons are highly fossiliferous (the remains of small mammals and gastropods) and show signs of paleosol formation, such as calcite nodules and crusts incorporating plant debris, and burrow structures (Harzhauser et al., 2017).

4.2 Bulk and clay mineralogy

The mineralogical composition of the Valley of Lakes samples is dominated by quartz (10 wt %–55 wt %), il-

lite/muscovite (10 wt %–50 wt %), calcite (0 wt %–70 wt%), feldspar (5 wt %–15 wt %; mainly albite and plagioclase and minor orthoclase) and hematite (0 wt %–10 wt %) (Table S1). XRD analysis identifies the illite/muscovite as an almost pure illitic phase composed of >95 % Ilt layers and <5 % Smc layers (Fig. S1) with the $1M_d$ polytype structure dominating (∼ 90 %–95 % of the total illite fraction; Fig. S2). The proportions of the 1M and $2M_1$ polytype structures of illite do not exceed ∼ 5 %–10 % of the total illite fraction. Kaolinite, chlorite (Mg-rich), mixed-layered Ilt–Smc comprised of ∼ 30 %–10 % Ilt layers and ∼ 70 %–90 % Smc layers (Fig. S1) as well as Ti-oxides (rutile and anatase) represent minor constituents (Fig. S2), together accounting for less than ∼ 5 wt % of the sediments. Trace amounts of zeolite and amphibole (<5 wt %) are documented between ∼ 35 and 45 m and between ∼ 90 and 110 m in the sedimentary succession respectively, i.e. adjacent to the basalt I and II groups. Vermiculite, dolomite, ankerite, anhydrite, halite and pyrite were not identified in the samples, which contrasts with observations made by Höck et al. (1999).

The sediments from the Tsagaan Ovoo Formation have the highest proportions of quartz, illite, feldspar and hematite and the lowest content of calcite compared with the other two formations, consistent with less abundant calcrete horizons developed in the upper-Eocene sediments (Fig. 3a). The sediments from the Oligocene Hsanda Gol and lower-Miocene Loh formations have highly variable but on average higher calcite contents than the Tsagaan Ovoo Formation due to abundant paleosol formation and related lower silicate mineral and hematite contents (Fig. 3b, c). The depletion of hematite in these samples argues for a detrital origin and for the precipitation of this mineral phase on silicate detritus during sediment transportation under oxic conditions. No systematic trends in the abundance of the mineral phases was observed across the investigated profile (see Table S1).

4.3 Microfabrics and illite crystallization ages

A microstructural study of weakly consolidated samples taken from the Hsanda Gol Formation reveals (sub)angular to rounded detrital quartz grains (Fig. S3a), which are partly overgrown by diagenetic quartz cement (Fig. S3b), as well as partially dissolved feldspar grains (Fig. S3c). Calichized areas are cemented by calcite spar, which appears as crypto- to microcrystalline material with aggregate particle sizes in the micrometre to millimetre range (Fig. S3d). All of these components are covered or intergrown by fine hematite particles (Fig. S3e), although silt-sized hematite grains are also observable. Coarse chlorite flakes as well as tiny, rounded to vermiform kaolinite particles are barely seen (Fig. S3f). Indeed, the clay mineral suite is dominated by two types of illite and one type of Ilt–Smc. SEM-EDX analysis suggests that the illites have higher contents of Al_2O_3 and K_2O, but lower contents of SiO_2 and Na_2O than the Ilt–Smc. The illites occur either as micrometre-sized particles with platy or pseudohexagonal forms being evenly dispersed throughout the matrix (type 1: Fig. 4a, c, e, g) or as long (micrometre-scale) but thin laths and fibres, which grow into the open pore space (type 2: Fig. 4b, d, f, g, h). The latter type of illite is often referred to as "hairy illite" (Güven et al., 1980; Rafiei et al., 2020). The Ilt–Smc is a nanometre-sized material with flaky to irregular particle forms, which covers detrital grains or grows into the open pore space (type 3: Fig. 4b, d, h).

When viewed together with the results of the illite polytype analysis and measured K–Ar ages (Table 1), all subsamples represent physical mixtures of detrital $2M_1$ illite/muscovite (type 1), authigenic $1M_d/1M$ illite (type 2) and authigenic $1M_d$ Ilt–Smc (type 3). Accordingly, the plot of the proportion of $2M_1$ illite/muscovite against the K–Ar age of a given subsample (Fig. 5) provides individual crystallization ages for the detrital and authigenic illitic phases (Grathoff and Moore, 1996): the upper intercept of the best-fitting line at 100 % of $2M_1$ reveals the crystallization age of detrital illite/muscovite, which is 727.6 to 797.9 Ma. The lower intercept of the best-fitting lines at 100 % of $1M_d + 1M$ gives crystallization ages for the authigenic clay minerals, which vary between 25.2 and 34.2 Ma.

4.4 Geochemistry and weathering indices

Variations in the major element composition of the samples (Table S2) follow changes in the abundance of silicate minerals (e.g. quartz, feldspar and clay minerals) relative to calcite and hematite across the sedimentary succession. No distinct trends among the different formations are seen, except for a lower CaO content and higher contents of SiO_2, Al_2O_3, K_2O, Na_2O, MgO and Fe_2O_3, on average, in the Tsagaan Ovoo Formation, compared with the Hsanda Gol and Loh formations, corroborating the mineralogical and petrographic results (see Table S1 and Fig. 3). Minor amounts of TiO_2 belong to rutile and anatase, and traces of MnO and P_2O_5 correspond to Mn oxides and apatite. The positive correlations of Cu, Ga, Rb and Zn with Al_2O_3 as well as Ce, La, Y and Zr with TiO_2 and Sr with CaO point to their association with clay minerals (i.e. structural incorporation or sorption onto the clay mineral surface), heavy minerals and carbonate minerals respectively (Abdullayev et al., 2021). Ba, Co, Cr, Hf, Nb, Ni, Pb, Sc, Th, V and U are inconspicuous due to the lack of a correlation with Al_2O_3 and TiO_2 or low concentration in the samples.

The plot of the chemical data in the A–CN–K ternary diagram (Fig. 6) shows that the samples fall within or plot slightly above the compositional range of post-Archean Australian shale (PAAS) and average Proterozoic shale (APS) and, thus, follow the predicted weathering trend for basalt protoliths and upper-continental-crust (UCC) rocks (Nesbitt and Young, 1984; Bahlburg and Dobrzinski, 2011). The shift of most of the data toward the K pole of the diagrams indicates that K-metasomatism has affected the chemical composition of the sediments through the growth of authigenic illite

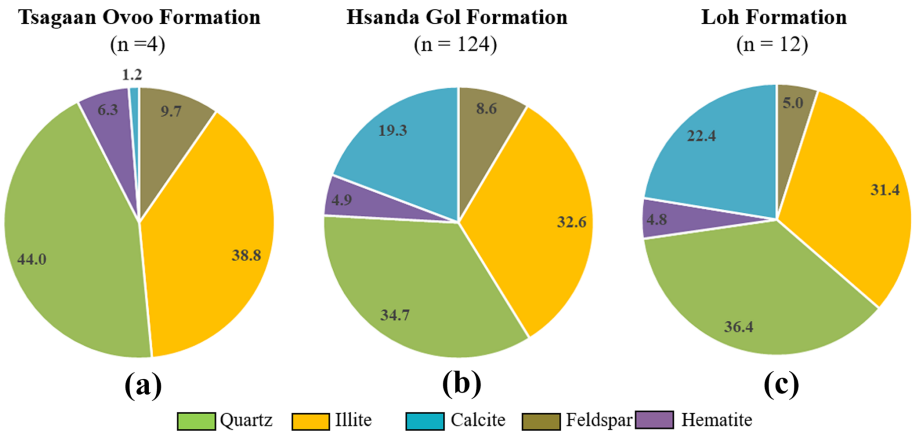

Figure 3. Averaged mineralogical composition (in wt %) of the sediments from the **(a)** upper-Eocene Tsagaan Ovoo Formation, **(b)** Oligocene Hsanda Gol Formation and **(c)** lower-Miocene Loh Formation from the Valley of Lakes, determined by XRD analysis.

Table 1. Compilation of illite polytype quantification and K–Ar ages of grain size subfractions of sediments collected from the TAT section (~ 90.5 m), TGR-C section (~ 78.0 m), SHG-D section (~ 55.5 m) and TGR-AB section (~ 35.0 m). The analytical error for the K–Ar age calculations is given as a 95 % confidence level (2σ). STP denotes standard temperature and pressure, and cps refers to count per second.

Sample	Size fraction [µm]	$A_{(-112)}$ [cps · 2θ]	1M [%]	$A_{(114)}$ [cps · 2θ]	$2M_1$ [%]	$1M_d$ [%]	K_2O [wt %]	^{40}Ar [nL/g] STP	^{40}Ar [%]	Age [Ma]	±2SD [Ma]
TAT	2–10	–	–	0.054	21	79	2.59	15.45	49.05	176.1	7.1
TAT	1–2	0.006	6	0.040	16	78	2.21	11.58	77.20	155.2	2.6
TAT	<1	0.012	7	0.023	10	83	3.39	10.75	38.18	95.8	3.2
TGR-C	2–10	–	–	0.038	16	84	2.68	13.98	81.46	155.1	2.9
TGR-C	1–2	–	–	0.031	13	87	3.64	15.80	76.96	129.6	2.4
TGR-C	<1	0.001	5	0.027	12	95	3.10	12.88	66.83	124.6	1.9
SHG-D	2–10	–	–	0.039	16	84	2.72	14.31	78.74	156.4	2.0
SHG-D	1–2	–	–	0.034	14	86	3.86	15.93	76.09	123.6	3.2
SHG-D	<1	0.011	6	0.016	8	94	3.49	10.38	70.94	89.9	1.3
TGR-AB	2–10	–	–	0.032	14	86	3.83	17.29	84.05	134.8	3.4
TGR-AB	1–2	–	–	0.027	12	88	3.97	16.63	84.33	125.3	1.8
TGR-AB	<1	0.032	9	–	0	91	0.64	0.70	10.52	33.9	3.2

and Ilt–Smc (Fedo et al., 1995), consistent with petrographic observations and clay polytype analyses. The CIA, CIW and PIA values vary from 70 to 83, 83 to 97 and 79 to 96 across the different formations, with averages of 79, 94 and 92 for the Loh Formation and 76, 90 and 88 for both the Hsanda Gol and Tsagaan Ovoo formations respectively (Table S3).

4.5 Soil carbonate $\delta^{18}O$ and $\delta^{13}C$ isotopic composition

The $\delta^{18}O$ and $\delta^{13}C$ values of the soil carbonates vary in the range from −11.7 ‰ to −0.2 ‰ and from −8.1 ‰ to −3.8 ‰ across the sedimentary succession of the Valley of Lakes (Table S4). Six samples taken close to the basalt I and II groups show comparatively lighter isotope values, −12.9 ‰ to −8.6 ‰ for $\delta^{18}O$ and −9.4 ‰ to −8.3 ‰ for $\delta^{13}C$, which indicates post-depositional overprinting. Therefore, these samples are not considered further. A high scatter in $\delta^{18}O$ values (−9.3 ‰ to −0.2 ‰) and relatively light $\delta^{13}C$ values (−7.5 ‰ to −6.4 ‰) are seen in the lower part of the Hsanda Gol Formation, changing into less fluctuating $\delta^{18}O$ values (−10.3 ‰ to −7.0 ‰) and systematically heavier $\delta^{13}C$ values (−7.6 ‰ to −3.8 ‰) in the middle and upper part of the Hsanda Gol Formation until the lower Miocene. Around the series/stage boundary, a gradual shift towards lighter $\delta^{18}O$ values (−11.7 ‰ to −8.6 ‰) and fluctuating but lighter $\delta^{13}C$ values (−8.1 ‰ to −4.4 ‰) are evident.

5 Discussion

5.1 Sediment provenance

The time interval from the Neoarchean to the late Permian saw the development of large parts of the fault- and thrust-bounded crystalline basement of Mongolia. The main lithological units forming this basement include Neoarchean metamorphic rocks and Palaeozoic metasediments and mag-

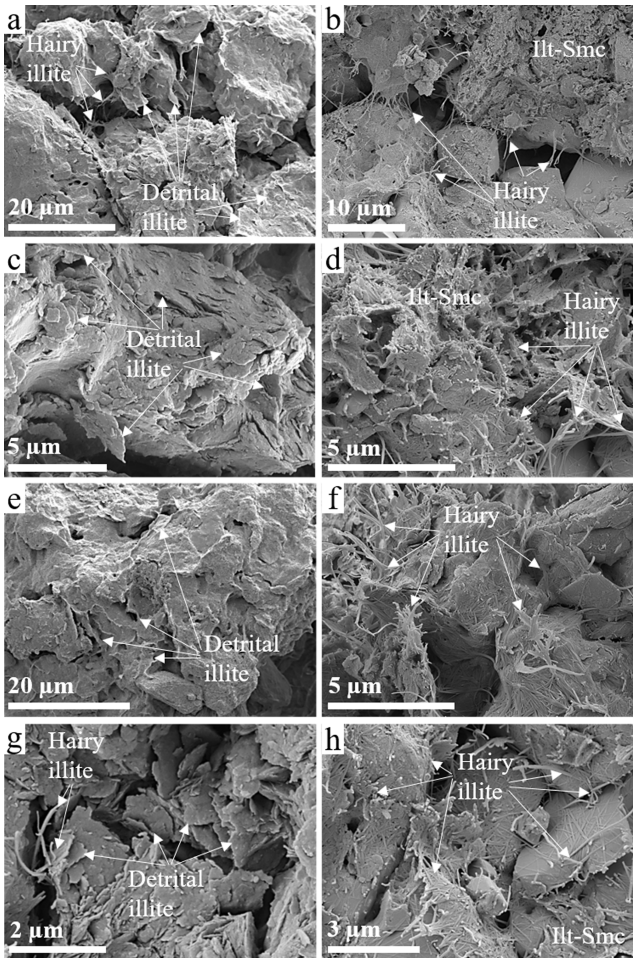

Figure 4. Secondary electron images of partly calichized and illitized silty to sandy deposits from the of the Oligocene Hsanda Gol Formation, Valley of Lakes, collected from the **(a–b)** TAT section (~ 90.5 m), **(c–d)** TGR-C section (~ 78.0 m), **(e–f)** SHG-D section (~ 55.5 m) and **(g–h)** TGR-AB section (~ 35.0 m). The detrital illite/muscovite **(a, c, e, g)** occurs as coarse, rounded or pseudohexagonal platelets, whereas authigenic illite–smectite (Ilt–Smc) and hairy illite **(b, d, f, h)** appear either as fine, flaky to irregular particles or as long but thin laths and fibres, both covering detrital grains or growing into the open pores.

matic rocks, which are all intruded by volcanic and magmatic rocks of various age, composition and provenance (Zorin et al., 1993). This complex architecture and the denudation processes in the Mesozoic, which formed the Valley of Lakes basin and created the present-day regional landscape and relief, are documented in the heavy mineral spectra of the Cenozoic basin fill (Höck et al., 1999): the presence of epidote, amphibole, garnet, rutile, pyroxene, sphene, zircon and tourmaline suggest that a mountainous region in the area of the present-day Khangai Mountains was the potential source area (McLennan et al., 1993). Quartz, pegmatite, granite, siltstone, basalt and carbonate clasts found in the gravel fraction (Höck et al., 1999) are also indicative of a heterogeneous provenance for the Valley of Lakes sediments.

The major oxide compositions of the sediments from the Valley of Lakes mainly plot in the "P4-quartzose sedimentary provenance" field, and only a few samples plot into the "P1-mafic igneous provenance" field in the Roser and Korsch (1988) discrimination diagram (Fig. 7). This indicates that metamorphosed sediments rich in quartz and poor in feldspar, and subordinate mafic to intermediate igneous and metamorphic rocks are the source rocks for the Valley of Lakes sediments. These rock types are common to all lithological units exposed in the adjacent lands of the Valley of Lakes (Höck et al., 1999). However, if considering the crystallization ages of the $2M_1$ detrital illite/muscovite (727.6 to 797.9 Ma; see Fig. 5), a robust assignment to provenance areas in the adjacent northern Burd Gol zone and Baidrag zone is possible. The Burd Gol zone dominantly hosts metapelites, metapsammites and metacherts, which have an age of 699 ± 35 Ma, as inferred from K–Ar dating of muscovite (Teraoka et al., 1996), which closely matches the detrital illite/muscovite ages measured in the sediments from the Valley of Lakes. The shift towards older ages can be explained by a minor contribution of Neoarchean rocks from the nearby Baidrag zone (~ 2.65 Ga old), which are comprised of high-grade gneisses, charnockites and amphibolites. Both source areas coincide with the heavy mineral spectra and gravel lithologies of the Valley of Lakes sediments (Höck et al., 1999).

Assuming that the detrital illite/muscovite in the Valley of Lakes sediments is a mixture of eroded, metamorphosed and intruded material from both source regions, a relative contribution of ~ >95 % from the Burd Gol zone and ~ <5 % from the Baidrag zone to the total detrital mica fraction can be calculated. Detrital silicate influx from the northernmost Bayan Khongor zone, Dzag zone and Khangai zone is considered to be unlikely, as these source areas are geologically younger (Ordovician to Cretaceous) (Teraoka et al., 1996). Mixtures of different proportions of detritus from the Burd Gol zone and some younger and older material are also unlikely, as constant source proportions over time would be required to explain the same ages for the four investigated samples. This assertion is consistent with the conclusion drawn by Richoz et al. (2017), who argued that the overall sedimentation system and the sediment provenance areas have not significantly changed in the considered time frame. Therefore, the source area relationships of the sediments from the Valley of Lakes are less complex than previously thought, with most detritus delivered from the regionally adjacent northern areas located within a 100 km range. Thus, variations in the chemical weathering indices outlined below most likely record changes in the weathering conditions of the source rock areas rather than changes in the sedimentary facies at the same time.

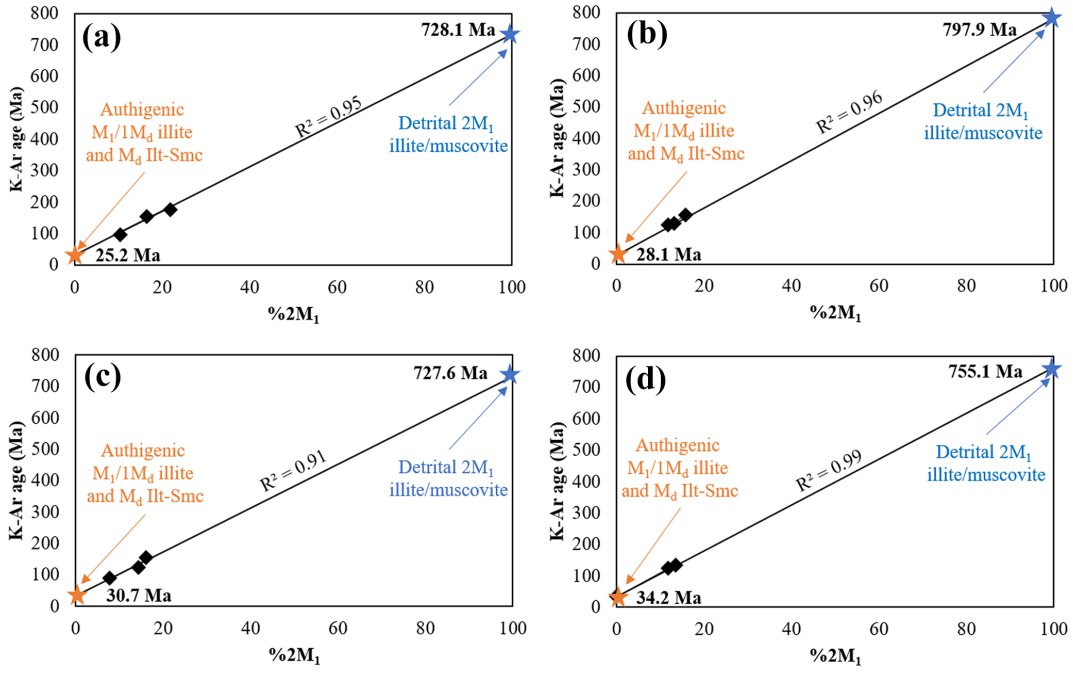

Figure 5. Crystallization ages of detrital $2M_1$ illite/muscovite and of authigenic $1M_d/1M$ illite and illite–smectite (Ilt–Smc) from the Valley of Lakes, calculated for sediments collected from the **(a)** TAT section (~ 90.5 m), **(b)** TGR-C section (~ 78.0 m), **(c)** SHG-D section (~ 55.5 m) and **(d)** TGR-AB section (~ 35.0 m) using illite polytype quantification and K–Ar age systematics of different grain size subfractions (from left to right: <1, 1–2 and 2–10 µm).

5.2 Depositional environment

The poorly sorted, massive to partly cross-bedded sand and gravel beds of the Tsagaan Ovoo Formation are interpreted as debris flow deposits in alluvial fans, according to the classification of Miall (1996) for fluvial sediments. These were generated during or soon after heavy rainfall events, which caused the water-saturated regolith to move downslope (Hubert and Filipov, 1989). The finer, laminated layers with ripple marks, inverse to normal grading and channel fills deposited between the coarser clastic beds represent the background sedimentation in the upper Eocene, i.e. braided river deposits developed in close vicinity to propagating alluvial fans (Miall, 1996). Imbrications of pebbles, cobbles and clasts within these beds suggest a palaeocurrent direction from north to south (Höck et al., 1999), which is consistent with major sediment source areas in the northern Burd Gol zone. In contrast to Badamgarav (1993) and Daxner-Höck et al. (2017), we found no petrographic-sedimentological evidence for lake or playa sedimentation in the upper-Eocene strata, which we attribute to the different sample types considered: while Badamgarav (1993) and Daxner-Höck et al. (2017) identified efflorescent salt crusts composed of halite, tepees and polygonal structures in some sedimentary layers, no such structures were observed in the paleosol horizons of the same age. However, the scatter in the $\delta^{18}O$ isotopic composition of the soil carbonates, which has been attributed to varying amounts of evaporation (Richoz et al., 2017), is consistent with a playa lake setting.

The poorly sorted, often horizontally bedded and fossiliferous clay–silt–sand(stone) beds of the Hsanda Gol Formation were deposited in a complex environment: the finer beds have likely been developed in ephemeral lakes or braided rivers systems draining proximal alluvial fans, as indicated by the presence of channel sand bodies with basal channel scour lags and cross-bedded sand fill. The sandier beds are interpreted as open-steppe deposits, which have been temporarily affected by ephemeral river and playa lake sedimentation (Miall, 1996), as can be inferred from occasional mud cracks and salt crusts (halite; Höck et al., 1999). On the contrary, Sun and Windley (2015) proposed an aeolian origin for the Oligocene sediments and interpreted them as loess deposits, which were transported by westerly winds, based on rare earth element (REE) patterns and comparison with grain size distributions obtained from recent loess deposits from Kansas (USA) and the Chinese Loess Plateau. Although we cannot exclude that long-distance transport and subsequent deposition of dust has contributed to at least a minor proportion of the total basin fill of the Valley of Lakes, we found no petrographic evidence for any aeolian influences, such as ripples, coarsening up laminae or climbing translatent strata, ventifacts, mud curls, or even quartz grains with crescentic percussion marks (Kenig, 2006; Z. Li et al., 2020).

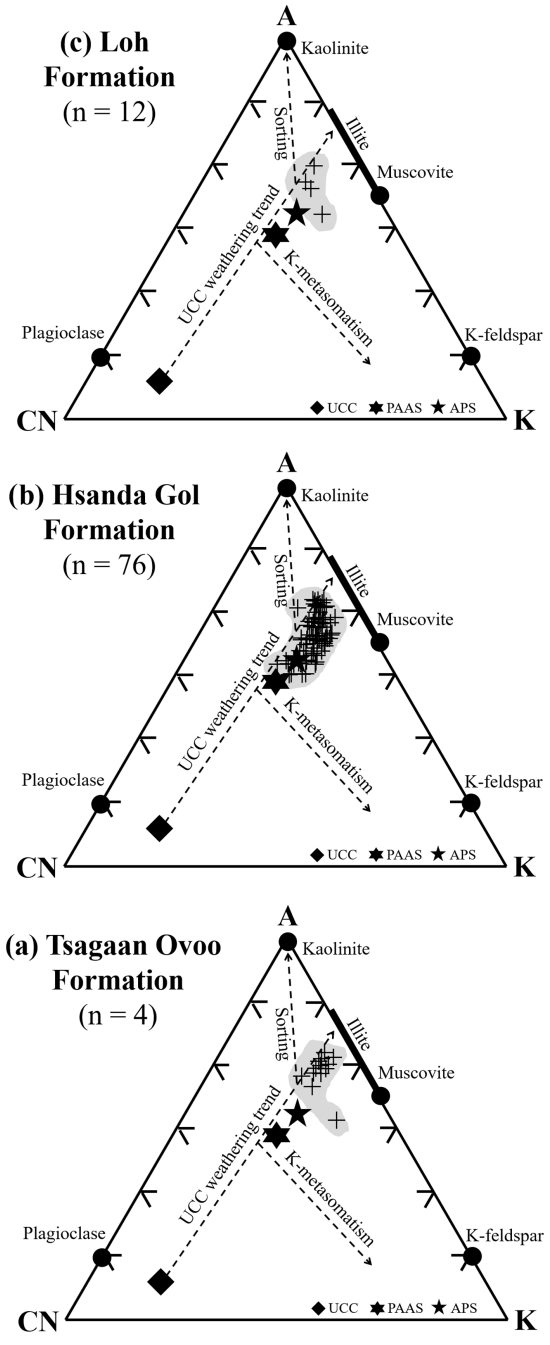

Figure 6. Al_2O_3 – ($CaO^* + Na_2O$) – K_2O (A–CN–K) ternary diagram of Nesbitt and Young (1984) showing the compositional ranges of sediments from the Valley of Lakes, from the bottom to the top, from **(a)** the upper-Eocene Tsagaan Ovoo Formation, **(b)** the Oligocene Hsanda Gol Formation and **(c)** the lower-Miocene Loh Formation. Note that most samples are shifted to the K pole of the diagram, which indicates a post-depositional enrichment of K_2O due to illitization. The composition of upper continental crust (UCC), average Proterozoic shale (APS) and post-Archean Australian shale (PAAS) are included for comparison.

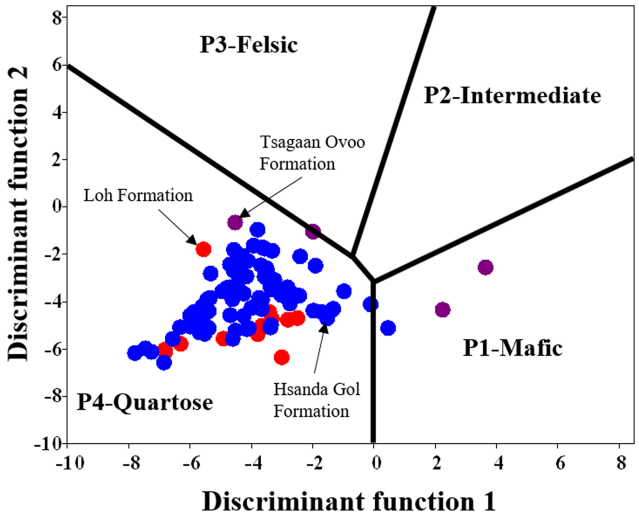

Figure 7. Discrimination plot of discriminant function 1 and 2 indicating a narrow provenance range (mainly type P4-quartzose) for the sediments from the Valley of Lakes, Mongolia.

The lithological variability of the Loh Formation (i.e. poorly sorted and highly fossiliferous clay–silt–sand–gravel beds deposited in alternate mode) can be best explained by a combination of debris flow deposits in alluvial fans (coarse clastic material) and abandoned channel deposits and waning flood sedimentation (fine clastic material) of a shallow, perennial flowing braided river system Miall (1996). Imbrication of gravels and flow structures in the basalt III group still indicate a palaeo-current direction from north to south (Höck et al., 1999), which suggests that the Burd Gol zone is the main source area at least up to the upper lower Miocene.

5.3 Origin of hairy illite and Ilt–Smc

Höck et al. (1999) and Sun and Windley (2015) proposed an aeolian origin or a coupled aeolian–fluviatile origin for the finest fraction of the Valley of Lakes sediments, whereas Richoz et al. (2017) concluded that the finest fraction is authigenic and was formed during or shortly after the flows of the different basalt groups. However, none of the above studies presented radiometric ages of the clay fraction to confirm their assertions. Our XRD and SEM study shows that the clay mineral fraction of the Oligocene Hsanda Gol Formation is dominated by hairy illite and subordinate flake-shaped Ilt–Smc, which cover detrital grains or grow into the pore space (Fig. 4). All of these features are typical for authigenic illitic phases (Güven et al., 1980; Rafiei et al., 2020). The polytype analysis and K–Ar age dating reveal that these illitic phases were precipitated between 34.2 and 25.2 Ma (Fig. 5), which (within uncertainty of the K–Ar age dating method used here) is well within the documented intrusion ages of the basalt I group (32.4–29.1 Ma) and basalt II group (28.7–

24.9 Ma) (Daxner-Höck et al., 2017) and closely matches the biozonation reported in Harzhauser et al. (2017).

The origin of Ilt–Smc in the Valley of Lakes sediments is difficult to constrain: it could have been formed during low-temperature pedogenesis from smectite or kaolinite precursors of "zero" age (Huggett et al., 2016), which were deposited due to wind (allochthonous clay source) or soil water (autochthonous source) action, through a dissolution–(re)precipitation mechanism. Pedogenic degradation of detrital illitic minerals to produce Ilt–Smc under acidic conditions at low temperature has also been observed (Meenakshi et al., 2020). On the contrary, several published studies have questioned a low-temperature origin of Ilt–Smc in sedimentary successions: Ilt–Smc found in paleosols from the Illinois Basin was shown to be the alteration product of siliceous parental phases, which interacted with hydrothermal brines generated during burial diagenesis rather than of ancient soil formation processes (McIntosh et al., 2020). Środoń (1984) concluded that smectite and Ilt–Smc phases are relatively stable in near-surface surroundings until the elevated temperatures of deep diagenesis are reached, which is consistent with slow kinetics of smectite illitization calculated for shallow buried sediments and low-temperature settings (Cuadros, 2006). In the case of the Valley of Lakes sediments, the relatively low Ilt content in Ilt–Smc ($\sim$ 10 %–30 % Ilt layers) and the stratigraphic age progression of the authigenic illitic phases up-section in the sedimentary succession may indicate a pedogenic origin of the Ilt–Smc.

In contrast to the Ilt–Smc, a pedogenic origin of the hairy illite is unlikely, as the formation of this mineral phase requires temperatures of around 100 °C (Güven et al., 1980; Nadeau et al., 1985; Baldermann et al., 2017), which is unrealistically high for a developing soil profile that has experienced a maximum burial depth of only a few hundred metres (Richoz et al., 2017). The high Ilt content (>95 % Ilt layers) and the hairy appearance of the illite argue for formation at elevated temperatures, which likely developed simultaneously or shortly after the prominent and recurrent basalt flows, consistent with a basalt-mediated diagenesis. Under such conditions, pore fluids rich in K^+, Al^{3+} and silicic acid are generated via the dissolution of unstable components, such as feldspar, which subsequently infiltrated the poorly consolidated (porous) Valley of Lakes sediments, thereby promoting the direct precipitation and growth of hairy illite in open pores (Fig. 4) and the hydrothermal alteration of pre-existing pedogenic Ilt–Smc to hairy illite (Baldermann et al., 2017). This mechanism is applicable to explain the shift of the chemical data towards the K pole in the A–CN–K ternary diagram (Fig. 6).

5.4 Palaeo-climate and weathering conditions

Climatic conditions are a primary control on the intensity and type of terrestrial weathering processes, where humid periods favour chemical weathering and arid periods favour physical weathering (Chamley, 1989). Analogously, hydroclimatic conditions are a key control on the intensity of pedogenic processes, which can be recorded in the $\delta^{13}C$ and $\delta^{18}O$ isotopic signature of authigenic carbonates (i.e. calcrete in paleosols), where wetter conditions favour an excursion towards lighter $\delta^{13}C$ and $\delta^{18}O$ values and drier conditions favour an excursion towards heavier $\delta^{13}C$ and $\delta^{18}O$ values (Richoz et al., 2017). Hence, variations in chemical weathering indicators (CIA, PIA and CIW) and in the $\delta^{13}C$ and $\delta^{18}O$ profiles of soil carbonates across a sedimentary succession can be used to trace and assess fluctuations in the climatic conditions that prevailed in the source areas and in the sedimentary basin at the time of sediment deposition as well as during pedogenesis (Nesbitt and Young, 1982; Bahlburg and Dobrzinski, 2011; Fischer-Femal and Bowen, 2021; Kelson et al., 2020; Zamanian et al., 2021). The formation of soil carbonates is a highly complex process that can complicate the interpretation of their $\delta^{13}C$ and $\delta^{18}O$ isotopic values (Richoz et al., 2017), as global climatic trends may be overprinted by regional factors, such as contamination by detrital carbonates, dolomitization, meteoric diagenesis, maturation or oxidation of organic matter, disequilibrium conditions between atmospheric (or biogenic) CO_2 and soil solution, evaporation, and basalt hydrothermalism (Kaufman and Knoll, 1995; Kent-Corson et al., 2009; Caves et al., 2014; Li et al., 2016; Baldermann et al., 2020; H. Li et al., 2020). However, considering that the vast majority of pristine soil carbonate $\delta^{13}C$ and $\delta^{18}O$ isotopic signatures are well preserved in the Valley of Lakes sediments, their use for palaeo-environmental reconstructions is possible.

The analysis of the $\delta^{13}C$ and $\delta^{18}O$ isotopic profiles recorded in the soil carbonates from the Valley of Lakes ($\sim$ 34–21 Ma) yielded the following palaeo-climatic trends, which are consistent with inverse shifts seen in the chemical weathering indices (dashed orange lines in Fig. 8), i.e. periods with increased precipitation coincide with higher chemical weathering indices and vice versa. This inverse relation is a robust indicator of changing humid/arid climatic conditions in an overall arid climate through the Cenozoic in Central Asia, considering that the source areas providing the silicate detritus have not changed over time in the investigated sedimentary succession and that a stable sedimentation system had been established. Thus, changes in the sedimentary facies, post-diagenetic impacts, basalt flow events or reginal tectonic activities are only barely seen in the soil carbonate $\delta^{13}C$ and $\delta^{18}O$ isotopic profiles. Accordingly, during the late Eocene to the earliest Oligocene, comparatively humid to semi-arid climatic conditions prevailed in Central Asia (phase i; biozone A to the bottom part of biozone B; $\sim$ 34–31 Ma); this was followed by an early Oligocene aridification (phase ii; bottom part of biozone B; $\sim$ 31 Ma) and the establishment of more arid climatic conditions afterwards until the terminal Oligocene (phase iii; upper part of biozone B to biozone C1-D; $\sim$ 31–23.5 Ma). A shift back towards comparatively humid to semi-arid climatic conditions is evident

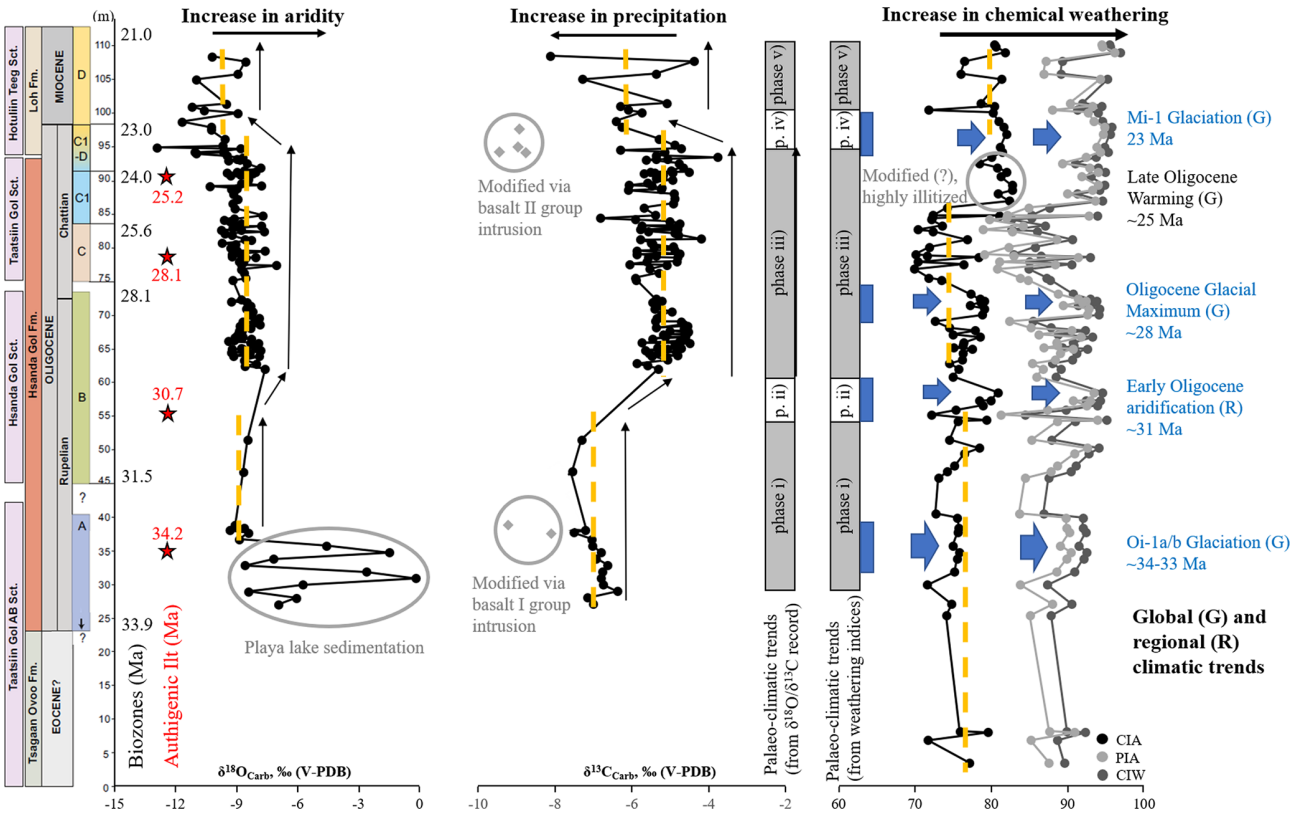

Figure 8. Lithostratigraphic framework of the sediments from the Valley of Lakes (Mongolia, Central Asia) showing the biozonation (modified after Harzhauser et al., 2017) and formation ages of the authigenic illitic (Ilt) phases obtained in this study (red asterisks), as well as soil carbonate $\delta^{18}O$ and $\delta^{13}C$ isotope profiles and shifts in the silicate mineral-derived chemical weathering indicators. Note that these hydroclimate proxies are inversely correlated and follow long-term trends (indicated by orange dashed lines) in aridification or increases in humidity in this region (indicated by black arrows). Increased chemical weathering degrees (highlighted using blue bars and blue arrows) coincide with glaciation events documented in time-equivalent marine deep-sea deposits (Zachos et al., 2001; Gallagher et al., 2020). Samples and intervals outlined by grey circles are most likely modified due to the flows of the basalt I and II groups or local strong illitization and are, therefore, excluded from the palaeo-climatic interpretation.

in the late Oligocene to earliest Miocene (phase iv; transition between biozones C1-D and D; ~ 23.5–23 Ma), which is followed by the establishment of these conditions in the early Miocene (phase v; biozone D; ~ 23–21 Ma). We note here that the atmospheric CO_2 concentration decreased from 800 to 200 ppm from ~ 33 to 22 Ma (Zhang et al., 2013), which should have shifted the soil carbonate $\delta^{13}C$ signatures towards lighter values. However, due to changes in aridification in Central Mongolia at the same time, this trend is not seen in the data. Indeed, an increase in aridification results in a restricted soil moisture content that can (i) increase the $\delta^{13}C$ value of soil carbonates; (ii) causes the plant productivity to decrease, which affects the ratio of atmospheric CO_2 to soil respired CO_2; and (iii) reduce the formation depth of the soil carbonates and, thus, the relative contributions of atmospheric CO_2 and soil-derived carbon (Cerling and Quade, 1993; Caves et al., 2014). As a consequence, the $\delta^{13}C$ isotopic signature of the soil carbonate is linked to aridification pulses, which also affect the weathering intensity of the sediment source areas, explaining the inverse relation between the isotope record and the chemical alteration indices. On the contrary, large changes in the $\delta^{18}O$ isotopic record of pristine soil carbonates are not to be expected given that the hydroclimatic variations are small in the semi-arid setting of the Valley of Lakes and that most moisture is recycled (Caves et al., 2015; Chamberlain et al., 2014; Kukla et al., 2019; Winnick et al., 2014).

Global cooling events established from $\delta^{13}C$ and $\delta^{18}O$ isotope records of marine deep-sea sediments (Zachos et al., 2001; Gallagher et al., 2020), such as the Oi-1a/b glaciation (~ 34–33 Ma) or the Oligocene glacial maximum (~ 28 Ma) are barely recorded in the soil carbonate $\delta^{13}C$ and $\delta^{18}O$ isotope profiles. However, they are visible in increases in chemical weathering indices at exactly these time intervals (blue bars and arrows in Fig. 8) and correspond to important faunal turnovers (Harzhauser et al., 2016). The early Oligocene aridification (~ 31 Ma) is seen by an excursion towards heavier isotopic values between ~ 55 and 60 m in the

rock record, but it does not correspond to an important faunal turnover (Harzhauser et al., 2016). On the contrary, the Oligocene warming event (~ 25 Ma), marked by an important extinction of the mammal community, is not seen in the $\delta^{13}C$ and $\delta^{18}O$ isotopic profiles. However, an increase in all chemical weathering indices is evident in the interval from ~ 87 to 92 m (upper part of Zone C1), which we attribute to strong illitization and local overprinting of the pristine chemical signature of these sediments. The following Mi-1 glaciation (~ 23 Ma) records high chemical weathering patterns but shows the expected excursion towards lighter $\delta^{13}C$ and $\delta^{18}O$ isotopic values.

The reasons for the Cenozoic climate change are hotly debated in the literature, but a strong decrease in atmospheric pCO_2 (Pagani et al., 2011; Anagnostou et al., 2016), major tectonic events, such as the collision of India with Asia and progressing exhumation of the Himalaya, as well as readjustments in oceanic gateway configurations are widely considered to have altered the global ocean–atmosphere circulation patterns (Caves Rugenstein and Chamberlain, 2018). This resulted in large-scale shifts in Earth's climate at this time, which are expressed, for example, in the formation and expansion of the Antarctica ice sheets and periods of intensified chemical weathering on land (Zachos et al., 2001, and references therein).

5.5 Hydroclimate and tectonic evolution in Central Asia

The links between the regional tectonic evolution and climate change in Central Asia have been extensively studied over the past decades. Recently, Caves Rugenstein and Chamberlain (2018) concluded that Central Asia has received moisture from the mid-latitude westerlies, maintaining stable semi-arid to arid climatic conditions ever since the early Eocene, based on the analysis of $\delta^{18}O$ and $\delta^{13}C$ isotope systematics of more than 7700 terrestrial authigenic carbonate samples from across Asia. On the contrary, southern Tibet, the central Tibetan Plateau, China and India dominantly received southerly monsoonal moisture, favouring more humid climatic conditions in these regions compared with Central Asia (Ingalls et al., 2018; Sandeep et al., 2018). Our data support this viewpoint: consistently higher $\delta^{18}O$ and $\delta^{13}C$ values measured for the soil carbonates from the Valley of Lakes (Fig. 8), compared with the surrounding regions, indicate that less precipitation and long-term, sustained arid climatic conditions prevailed in the late Eocene until the early Miocene (Cerling and Quade, 1993; Kent-Corson et al., 2009; Takeuchi et al., 2010; Caves et al., 2015; Li et al., 2016; Caves Rugenstein and Chamberlain, 2018). An influence of the height and extension of the Tibetan Plateau or the retreat of the Paratethys on the hydroclimate in Central Asia at this time (An et al., 2001; Zhang et al., 2009) is barely documented in the sedimentary record of the Valley of Lakes, although it cannot be excluded, which would be expressed in monsoon-dominant environmental pattern and varying amounts of precipitation (Zhang et al., 2013).

The increase in the $\delta^{13}C$ values of the soil carbonates in the Oligocene and the decrease in the $\delta^{18}O$ values in the terminal Oligocene are ultimately linked to coupled effects arising from the Cenozoic global cooling and the uplift of the Tian Shan and Altai from the early Neogene onward, which caused changes in the seasonality and quantity of precipitation (Hendrix et al., 1994; Macaulay et al., 2016; Hellwig et al., 2017; Wang et al., 2020). The resultant effects on the fractionation of $\delta^{18}O$ and $\delta^{13}C$ isotopes in soil carbonates are detailed in Caves Rugenstein and Chamberlain (2018) but are directly related to the development and the establishment of the Altai rain shadow front. As a consequence, on the leeward side of the Altai, sustained, long-term drying occurred, which is expressed by systematic changes seen in the isotope profiles and chemical weathering indices (Fig. 8). Moreover, the progressive uplifting of the Hangay Mountains to the north from the early Oligocene also blocked Siberian moisture transport to the northern Gobi (as can be inferred from $\delta^{13}C$ and $\delta^{18}O$ isotope signatures recorded in paleosol carbonates from different transects at the northern edge of the Gobi Desert and in the lee of the Altai and Hangay Mountains) and, consequently, contributed to the aridification of this area (Caves et al., 2014; Sahagian et al., 2016; McDannell et al., 2018). This aridification led to a concurrent extension of the Gobi Desert, causing shifts and turnovers in mammalian and gastropod assemblages observed in soils of western Mongolia and in the adjacent eastern Valley of Lakes basin at this time (Neubauer et al., 2013; Harzhauser et al., 2017; Barbolini et al., 2020). We conclude that the climatic and environmental evolution of Central Asia in the Cenozoic was closely coupled to global climate change, regional tectonic events and adaptions of the circulation pattern of the westerly winds, transporting less moisture to continental Mongolia, which favoured aridification.

Code and data availability. The data used in the paper can be accessed at https://zenodo.org/record/5521410#.YUsyfX2xU-U (Baldermann et al., 2021b). XRD, XRF, TIC, and $\delta^{13}C$ and $\delta^{18}O$ isotope data are also provided in the Supplement.

Supplement. The supplement related to this article is available online at: https://doi.org/10.5194/cp-17-1955-2021-supplement.

Author contributions. AB wrote the paper. WEP carried out field work and collected the samples. OW and SR provided the mineralogical and geochemical data. EA conducted the discriminant function analyses. KW provided the K–Ar ages. AB, SB, SL, WEP, MR and SR characterized the palaeo-environment and interpreted the stable $\delta^{13}C$ and $\delta^{18}O$ isotope records. All authors contributed to writing the paper.

Competing interests. The authors declare that they have no conflict of interest.

Acknowledgements. The authors acknowledge Maria Hierz, Judith Jernej, Silvia Perchthold and Andrea Wolf (Graz University of Technology) and Sanja Šimic (Institute for Electron Microscopy and Nanoanalysis and Graz Centre for Electron Microscopy), who assisted us with the preparation and analysis of the samples. Jose R. Quezada-Hinojosa is greatly acknowledged for drawing the lithostratigraphic profile and for providing the oxygen and carbon isotopic data. This research was funded by the NAWI Graz Geocenter (Graz University of Technology). Field work and sample acquisition were supported by the Austrian Science Fund (FWF; grant no. P-23061-N19 to Gudrun Daxner-Höck). We thank our Mongolian and European team members for manifold support during the field work.

Financial support. This research has been supported by the Austrian Science Fund (grant no. P-23061-N19) and the TU Graz, Internationale Beziehungen und Mobilitätsprogramme (grant no. NAWI Graz Geocenter).

Review statement. This paper was edited by Zhengtang Guo and reviewed by Jeremy Caves Rugenstein and Chunxia Zhang.

References

Abdullayev, E., Baldermann, A., Warr, L. N., Grathoff, G., and Taghiyeva, Y.: New constraints on the palaeo-environmental conditions of the Eastern Paratethys: Implications from the Miocene Diatom Suite (Azerbaijan), Sed. Geol., 411, 105794, https://doi.org/10.1016/j.sedgeo.2020.105794, 2021.

An, Z., Kutzbach, J. E., Prell, W. L., and Porter, S. C.: Evolution of Asian monsoons and phased uplift of the Himalaya-Tibetan plateau since Late Miocene times, Nature, 411, 62–66, https://doi.org/10.1038/35075035, 2001.

Anagnostou, E., John, E. H., Edgar, K. M., Foster, G. L., Ridgwell, A., Inglis, G. N., Pancost, R. D., Lunt, D. J., and Pearson, P. N.: Changing atmospheric CO_2 concentration was the primary driver of early Cenozoic climate, Nature, 533, 380–384, https://doi.org/10.1038/nature17423, 2016.

Badamgarav, D.: A brief lithologo-genetic characteristics of Eocene-Oligocene and Miocene deposits of the Valley of Lakes and Begger depression, in: International Geological Correlation Programme, Project 326 Oligocene-Miocene Transitions in the Northern Hemisphere, Excursion Guide-Book Mongolia: Oligocene-Miocene Boundary in Mongolia, edited by: Barsbold, R. and Akhmetiev, M. A., International Geological Correlation Programme, Mongolia, 36–39, 1993.

Bahlburg, H. and Dobrzinski, N.: A review of the Chemical Index of Alteration (CIA) and its application to the study of Neoproterozoic glacial deposits and climate transitions, in: The Geological Record of Neoproterozoic Glaciations, edited by: Arnaud, E., Halverson, G. P., and Shields-Zhou, G., Chapter 6, Geol. Soc. Lond. Mem., 36, 81–92, https://doi.org/10.1144/M36.6, 2011.

Baldermann, A., Grathoff, G. H., and Nickel, C.: Micromilieu controlled glauconitization in fecal pellets at Oker (Central Germany), Clay Miner., 47, 513–538, https://doi.org/10.1180/claymin.2012.047.4.09, 2012.

Baldermann, A., Dohrmann, R., Kaufhold, S., Nickel, C., Letofsky-Papst, I., and Dietzel, M.: The Fe-Mg-saponite solid solution series – a hydrothermal synthesis study, Clay Miner., 49, 391–415, https://doi.org/10.1180/claymin.2014.049.3.04, 2014.

Baldermann, A., Dietzel, M., Mavromatis, V., Mittermayr, F., Warr, L. N., and Wemmer, K.: The role of Fe on the formation and diagenesis of interstratified glauconite-smectite and illite-smectite: A case study of Upper Cretaceous shallow-water carbonates, Chem. Geol., 453, 21–34, https://doi.org/10.1016/j.chemgeo.2017.02.008, 2017.

Baldermann, A., Mittermayr, F., Bernasconi, S. M., Dietzel, M., Grengg, C., Hippler, D., Kluge, T., Leis, A., Lin, K., Wang, X., Zünterl, A., and Boch, R.: Fracture dolomite as an archive of continental palaeo-environmental conditions, Commun. Earth Environ., 1, 35, https://doi.org/10.1038/s43247-020-00040-3, 2020.

Baldermann, A., Reinprecht, V., and Dietzel, M.: Chemical weathering and progressing alteration as possible controlling factors for creeping landslides, Sci. Total Environ., 778, 146300, https://doi.org/10.1016/j.scitotenv.2021.146300, 2021a.

Baldermann, A., Wasser, O., Abdullayev, E., Bernasconi, S., Löhr, S. C., Wemmer, K., Piller, W. E., Rudmin, M., and Richoz, S.: Palaeo-environmental evolution of Central Asia during the Cenozoic, Zenodo [data set], available at: https://zenodo.org/record/5521410#.YUsyfX2xU-U, last access: 26 September 2021b.

Barbolini, N., Woutersen, A., Dupont-Nivet, G., Silvestro, D., Tardif, D., Coster, P. M. C., Meijer, N., Chang, C., Zhang, H.-X., Licht, A., Rydin, C., Koutsodendris, A., Han, F., Rohrmann, A., Liu, X.-J., Zhang, Y., Donnadieu, Y., Fluteau, F., Ladant, J.-B., Le Hir, G., and Hoorn, C.: Cenozoic evolution of the steppe-desert biome in Central Asia, Sci. Adv., 6, eabb8227, https://doi.org/10.1126/sciadv.abb8227, 2020.

Bosboom, R., Dupont-Nivet, G., Grothe, A., Brinkhuis, H., Villa, G., Mandic, O., Stoica, M., Huang, W., Yang, W., Guo, Z., and Krijgsman, W.: Linking Tarim sea retreat (west China) and Asian aridification in the late Eocene, Basin Res., 26, 621–640, https://doi.org/10.1111/bre.12054, 2014.

Caves, J. K., Sjostrom, D. J., Mix, H. T., Winnick, M. J., and Chamberlain, C. P.: Aridification of Central Asia and uplift of the Altai and Hangay Mountains, Mongolia: stable isotope evidence, Am. J. Sci., 314, 1171–1201, https://doi.org/10.2475/08.2014.01, 2014.

Caves, J. K., Winnick, M. J., Graham, S. A., Sjostrom, D. J., Mulch, A., and Chamberlain, C. P.: Role of the westerlies in Central Asia climate over the Cenozoic, Earth Planet. Sci. Lett., 428, 33–43, https://doi.org/10.1016/j.epsl.2015.07.023, 2015.

Caves Rugenstein, J. K. and Chamberlain, C. P.: The evolution of hydroclimate in Asia over the Cenozoic: A stable-isotope perspective, Earth-Sci. Rev., 185, 1129–1156, https://doi.org/10.1016/j.earscirev.2018.09.003, 2018.

Cerling, T. and Quade, J.: Stable carbon and oxygen isotopes in soil carbonates, in: Climate Change in Continental Isotopic Records, edited by: Swart, P., Lohmann, K., McKenzie, J., and Savin, S., American Geophysical Union, Geophysical Monograph, 78, 217–231, https://doi.org/10.1029/GM078p0217, 1993.

Cerling, T. E.: Late Cenozoic Vegetation Change, Atmospheric CO_2, and Tectonics, in: Tectonic Uplift and Climate Change, edited by: Ruddiman, W. F., Springer, Boston, MA, 313–327, https://doi.org/10.1007/978-1-4615-5935-1_13, 1993.

Cermeño, P., Falkowski, P. G., Romero, O. E., Schaller, M. F., and Vallina, S. M.: Continental erosion and the Cenozoic rise of marine diatoms, P. Natl. Acad. Sci. USA, 112, 4239–4244, https://doi.org/10.1073/pnas.1412883112, 2015.

Chamberlain, C. P., Winnick, M. J., Mix, H. T., Chamberlain, S. D., and Maher, K.: The impact of Neogene grassland expansion and aridification on the isotopic composition of continental precipitation, Global Biogeochem. Cy., 28, 992–1004, https://doi.org/10.1002/2014GB004822, 2014.

Chamley, H.: Clay Formation Through Weathering, in: Clay Sedimentology, Springer, Berlin, Heidelberg, Germany, 21–50, https://doi.org/10.1007/978-3-642-85916-8_2, 1989.

Cuadros, J.: Modeling of smectite illitization in burial diagenesis environments, Geochim. Cosmochim. Ac., 70, 4181–4195, https://doi.org/10.1016/j.gca.2006.06.1372, 2006.

Daxner-Höck, G., Badamgarav, D., Barsbold, R., Bayarmaa, B., Erbajeva, M., Göhlich, U. B., Harzhauser, M., Höck, V., Höck, E., Ichinnorov, N., Khand, Y., Lopez-Guerrero, P., Maridet, O., Neubauer, T., Oliver, A., Piller, W. E., Tsogtbaatar, K., and Ziegler, R.: Oligocene stratigraphy across the Eocene and Miocene boundaries in the Valley of Lakes (Mongolia), in: The Valley of Lakes in Mongolia, a key area of Cenozoic mammal evolution and stratigraphy, edited by: Daxner-Höck, G. and Göhlich, U., Paleobiodivers. Paleoenviron., 97, 111–218, https://doi.org/10.1007/s12549-016-0257-9, 2017.

Dupont-Nivet, G., Krijgsman, W., Langereis, C. G., Abels, H. A., Dai, S., and Fang, X. M.: Tibetan plateau aridification linked to global cooling at the Eocene-Oligocene transition, Nature, 445, 635–638, https://doi.org/10.1038/nature05516, 2007.

Fedo, C. M., Nesbitt, H. W., and Young, G. M.: Unraveling the effects of potassium metasomatism in sedimentary rocks and paleosols, with implications of paleoweathering conditions and provenance, Geology, 23, 921–924, https://doi.org/10.1130/0091-7613(1995)023<0921:UTEOPM>2.3.CO;2, 1995.

Fischer-Femal, B. J. and Bowen, G. J.: Coupled carbon and oxygen isotope model for pedogenic carbonates, Geochim. Cosmochim. Ac., 294, 126–144, https://doi.org/10.1016/j.gca.2020.10.022, 2021.

Gallagher, S. J., Wade, B., Qianyu, L., Holdgate, G. R., Bown, P., Korasidis, V. A., Scher, H., Houben, A. J. P., McGowran, B., and Allan, T.: Eocene to Oligocene high paleolatitude neritic record of Oi-1 glaciation in the Otway Basin southeast Australia, Glob. Planet. Change, 191, 103218, https://doi.org/10.1016/j.gloplacha.2020.103218, 2020.

Grathoff, G. H. and Moore, D. M.: Illite Polytype Quantification Using Wildfire© Calculated X-Ray Diffraction Patterns, Clays Clay Miner., 44, 835–842, https://doi.org/10.1346/CCMN.1996.0440615, 1996.

Guo, Z. T., Sun, B., Zhang, Z. S., Peng, S. Z., Xiao, G. Q., Ge, J. Y., Hao, Q. Z., Qiao, Y. S., Liang, M. Y., Liu, J. F., Yin, Q. Z., and Wei, J. J.: A major reorganization of Asian climate by the early Miocene, Clim. Past, 4, 153–174, https://doi.org/10.5194/cp-4-153-2008, 2008.

Güven, N., Hower, W. F., and Davies, D. K.: Nature of authigenic illites in sandstone reservoirs, J. Sed. Res., 50, 761–766, https://doi.org/10.1306/212F7ADB-2B24-11D7-8648000102C1865D, 1980.

Harzhauser, M., Daxner-Höck, G., López-Guerrero, P., Maridet, O., Oliver, A., Piller, W. E., Richoz, S., Erbajeva, M. A., and Göhlich, U. B.: The stepwise onset of the Icehouse world and its impact on Oligocene-Miocene Central Asian mammal communities, Sci. Rep., 6, 36169, https://doi.org/10.1038/srep36169, 2016.

Harzhauser, M., Daxner-Höck, G., Erbajeva, M. A., López-Guerrero, P., Maridet, O., Oliver, A., Piller, W. E, Göhlich U. B., and Ziegler, R.: Oligocene and early Miocene biostratigraphy of the Valley of Lakes in Mongolia, in: The Valley of Lakes in Mongolia, a key area of Cenozoic mammal evolution and stratigraphy, edited by: Daxner-Höck, G. and Göhlich, U., Palaeobiodivers. Palaeoenviron., 97, 219–231, https://doi.org/10.1007/s12549-016-0264-x, 2017.

Hellwig, A., Voigt, S., Mulch, A., Frisch, K., Bartenstein, A., Pross, J., Gerdes, A., and Voigt, T.: Late Oligocene–early Miocene humidity change recorded in terrestrial sequences in the Ili Basin (south-eastern Kazakhstan, Central Asia), Sedimentology, 65, 517–539, https://doi.org/10.1111/sed.12390, 2017.

Hendrix, M., Dumitru, T., and Graham, S.: Late Oligocene-early Miocene unroofing in the Chinese Tian Shan: An early effect of the India-Asia collision, Geology, 22, 487–490, https://doi.org/10.1130/0091-7613(1994)022<0487:LOEMUI>2.3.CO;2, 1994.

Höck, V., Daxner-Höck, G., Schmid, H. P., Badamgarav, D., Frank, W., Furtmüller, G., Montag, O., Barsbold, R., Khand, Y., and Sodov, J.: Oligocene-Miocene sediments, fossils and basalt from the Valley of Lakes (Central Mongolia) – an integrated study, Mitt. Österr. Geol. Ges., 90, 83–125, 1999.

Houben, A. J. P., Bijl, P. K., Pross, J., Bohaty, S. M., Passchier, S., Stickley, C. E., Röhl, U., Sugisaki, S., Tauxe, L., van de Flierdt, T., Olney, M., Sangiorgi, F., Sluijs, A., Escutia, C., and Brinkhuis, H. et al.: Reorganization of Southern Ocean plankton ecosystem at the onset of Antarctic glaciation, Science, 340, 341–344, https://doi.org/10.1126/science.1223646, 2013.

Hubert, J. F. and Filipov, A. J.: Debris-flow deposits in alluvial fans on the west flank of the White Mountains, Owens Valley, California, U.S.A., Sed. Geol., 61, 177–205, https://doi.org/10.1016/0037-0738(89)90057-2, 1989.

Huggett, J., Cuadros, J., Gale, A. S., Wray, D., and Adetunji, J.: Low temperature, authigenic illite and carbonates in a mixed dolomite-clastic lagoonal and pedogenic setting, Spanish Central System, Spain. Appl. Clay Sci., 132–133, 296–312, https://doi.org/10.1016/j.clay.2016.06.016, 2016.

Ingalls, M., Rowley, D. B., Olack, G., Currie, B. S., Li, S., Schmidt, J. L., Tremblay, M. M., Polissar, P. J., Shuster, D. L., Lin, D., and Colman, A. S.: Paleocene to Pliocene high elevation of southern Tibet: Implications for tectonic models of India-Asia collision, Cenozoic climate, and geochemical weathering, Geol. Soc. Am. Bull., 130, 307–330, https://doi.org/10.1130/B31723.1, 2018.

Kaufman, A. J. and Knoll, A. H.: Neoproterozoic variations in the C-isotopic composition of seawater: stratigraphic and biogeochemical implications, Precambrian Res., 73, 27–49, https://doi.org/10.1016/0301-9268(94)00070-8, 1995.

Kelson, J. R., Huntington, K. W., Breecker, D. O., Burgener, L. K., Gallagher, T. M., Hoke, G. D., and Petersen, S. V.: A proxy for all seasons? A synthesis of clumped isotope data from Holocene soil carbonates, Quat. Sci. Rev., 234, 106259, https://doi.org/10.1016/j.quascirev.2020.106259, 2020.

Kenig, K.: Surface microtextures of quartz grains from Vistulian loesses from selected profiles of Poland and some other countries, Quat. Int., 152–153, 118–135, https://doi.org/10.1016/j.quaint.2005.12.015, 2006.

Kent-Corson, M. L., Ritts, B. D., Zhuang, G., Bovet, P. M., Graham, S. A., and Chamberlain, C. P.: Stable isotopic constraints on the tectonic, topographic, and climatic evolution of the northern margin of the Tibetan Plateau, Earth Planet. Sc. Lett., 282, 158–166, https://doi.org/10.1016/j.epsl.2009.03.011, 2009.

Komar, N. and Zeebe, R. E.: Reconciling atmospheric CO_2, weathering, and calcite compensation depth across the Cenozoic, Sci. Adv., 7, eabd4876, https://doi.org/10.1126/sciadv.abd4876, 2021.

Kukla, T., Winnick, M. J., Maher, K., Ibarra, D. E., and Chamberlain, C. P.: The Sensitivity of Terrestrial $\delta^{18}O$ Gradients to Hydroclimate Evolution, J. Geophys. Res.-Atmos., 124, 563–582, https://doi.org/10.1029/2018JD029571, 2019.

Lear, C. H., Bailey, T. R., Pearson, P. N., Coxall, H. K., and Rosenthal, Y.: Cooling and ice growth across the Eocene-Oligocene transition, Geology, 36, 251–254, https://doi.org/10.1130/G24584A.1, 2008.

Li, B., Sun, D., Wang, X., Zhang, Y., Hu, W., Wang, F., Li, Z., Ma, Z., and Liang, B.: $\delta^{18}O$ and $\delta^{13}C$ records from a Cenozoic sedimentary sequence in the Lanzhou Basin, Northwestern China: implications for palaeoenvironmental and palaeoecological changes, J. Asian Earth Sci., 125, 22–36, https://doi.org/10.1016/j.jseaes.2016.05.010, 2016.

Li, H., Liu, X., Tripati, A., Feng, S., Elliott, B., Whicker, C., Arnold, A., and Kelley, A. M.: Factors controlling the oxygen isotopic composition of lacustrine authigenic carbonates in Western China: implications for paleoclimate reconstructions, Sci. Rep., 10, 16370, https://doi.org/10.1038/s41598-020-73422-4, 2020.

Li, Z., Yu, X., Dong, S., Chen, Q., and Zhang, C.: Microtextural features on quartz grains from eolian sands in a subaqueous sedimentary environment: A case study in the hinterland of the Badain Jaran Desert, Northwest China, Aeolian Res., 43, 100573, https://doi.org/10.1016/j.aeolia.2020.100573, 2020.

Lu, H., Wang, X., Wang, X., Chang, X., Zhang, H., Xu, Z., Zhang, W., Wei, H., Zhang, X., Yi, S., Zhang, W., Feng, H., Wang, Y., Wang, Y., and Han, Z.: Formation and evolution of Gobi Desert in central and eastern Asia, Earth-Sci. Rev., 194, 251–263, https://doi.org/10.1016/j.earscirev.2019.04.014, 2019.

Macaulay, E. A., Sobel, E. R., Mikolaichuk, A., Wack, M., Gilder, S. A., Mulch, A., Fortuna, A. B., Hynek, S., and Apayarov, F.: The sedimentary record of the Issyk Kul basin, Kyrgyzstan: climatic and tectonic inferences, Basin Res., 28, 57–80, https://doi.org/10.1111/bre.12098, 2016.

McDannell, K. T., Zeitler, P. K., and Idleman, B. D.: Relict Topography Within the Hangay Mountains in Central Mongolia: Quantifying Long-Term Exhumation and Relief Change in an Old Landscape, Tectonics, 37, 2531–2558, https://doi.org/10.1029/2017TC004682, 2018.

McIntosh, J. A., Tabor, N. J., and Rosenau, A. A.: Mixed-Layer Illite-Smectite in Pennsylvanian-Aged Paleosols: Assessing Sources of Illitization in the Illinois Basin, Minerals, 11, 108 , https://doi.org/10.3390/min11020108, 2020.

McLennan, S. M.: Weathering and Global Denudation, J. Geol., 101, 100th Anniversary Symposium: Evolution of the Earth's Surface, 295–303, available at: https://www.jstor.org/stable/30081153 (last access: 2 June 2021), 1993.

Meenakshi, Shrivastava, J. P., and Chandra, R.: Pedogenically degenerated illite and chlorite lattices aid to palaeoclimatic reconstruction for chronologically constrained (8–130 ka) loess-palaeosols of Dilpur Formation, Kashmir, India, Geosci. Front., 11, 1353–1367, https://doi.org/10.1016/j.gsf.2019.11.007, 2020.

Miall, A. D.: The Geology of Fluvial Deposits, Springer, Berlin, Germany, 1–598, https://doi.org/10.1007/978-3-662-03237-4?nosfx=y, 1996.

Mudelsee, M., Bickert, T., Lear, C. H., and Lohmann, G.: Cenozoic climate changes: A review based on time series analysis of marine benthic $\delta^{18}O$ records, Rev. Geophys., 52, 333–374, https://doi.org/10.1002/2013RG000440, 2014.

Mutz, S. G., Ehlers, T. A., Werner, M., Lohmann, G., Stepanek, C., and Li, J.: Estimates of late Cenozoic climate change relevant to Earth surface processes in tectonically active orogens, Earth Surf. Dynam., 6, 271–301, https://doi.org/10.5194/esurf-6-271-2018, 2018.

Nadeau, P. H., Wilson, M. J., McHardy, W. J., and Tait, J. M.: The conversion of smectite to illite during diagenesis: evidence from some illitic clays from bentonites and sandstones, Mineral. Mag., 49, 393–400, https://doi.org/10.1180/minmag.1985.049.352.10, 1985.

Neubauer, T. A., Harzhauser, M., Daxner-Höck, G., and Piller, W. E.: New data on the terrestrial gastropods from the Oligocene-Miocene transition in the Valley of Lakes, Central Mongolia, Paleontol. J., 47, 374–385, https://doi.org/10.1134/S003103011304014X, 2013.

Nesbitt, H. W. and Young, G. M.: Early Proterozoic climate and plate motions inferred from major element chemistry of lutites, Nature, 299, 715–717, https://doi.org/10.1038/299715a0, 1982.

Nesbitt, H. W. and Young, G. M.: Prediction of some weathering trends of plutonic and volcanic rocks based on thermodynamic and kinetic considerations, Geochim. Cosmochim. Ac., 48, 1523–1534, https://doi.org/10.1016/0016-7037(84)90408-3, 1984.

Norris, R., Turner, S. K., Hull, P. M., and Ridgwell, A.: Marine Ecosystem Responses to Cenozoic Global Change, Science, 341, 492–498, https://doi.org/10.1126/science.1240543, 2013.

Pagani, M., Huber, M., Liu, Z., Bohaty, S. M., Henderiks, J., Sijp, W. P., Krishnan, S., and DeConto, R. M.: The Role of Carbon Dioxide During the Onset of Antarctic Glaciation, Science, 334, 6060, 1261–1264, https://doi.org/10.1126/science.1203909, 2011.

Pälike, H., Norris, R. D., Herrle, J. O., Wilson, P. A., Coxall, H. K., Lear, C. H., Shackleton, N. J., Tripati, A. K., and Wade, B. S.: The heartbeat of the Oligocene climate system, Science, 314, 1894–1898, https://doi.org/10.1126/science.1133822, 2006.

Porter, T. M.: The geology, structure and mineralisation of the Oyu Tolgoi porphyry copper-gold-molybdenum deposits, Mongolia: A review, Geosci. Front., 7, 375–407, https://doi.org/10.1016/j.gsf.2015.08.003, 2016.

Rafiei, M., Löhr, S., Baldermann, A., Webster, R., and Kong, C.: Quantitative petrographic differentiation of detrital vs diagenetic clay minerals in marine sedimentary sequences: Implications for the rise of biotic soils, Precambrian Res., 350, 105948, https://doi.org/10.1016/j.precamres.2020.105948, 2020.

Richoz, S., Baldermann, A., Frauwallner, A., Harzhauser, M., Daxner-Höck, G., Klammer, D., and Piller, W. E.: Geochemistry and mineralogy of the Oligo-Miocene sediments of the Valley of Lakes, Mongolia, Palaeobiodivers. Palaeoenviron., 97, 233–258, https://doi.org/10.1007/s12549-016-0268-6, 2017.

Roser, B. P. and Korsch, R. J.: Provenance signatures of sandstone-mudstone suites determined using discriminant function analysis of major-element data, Chem. Geol., 67, 119–139, https://doi.org/10.1016/0009-2541(88)90010-1, 1988.

Sahagian, D., Proussevitch, A., Ancuta, L. D., Idleman, B. D., and Zeitler, P. K.: Uplift of Central Mongolia Recorded in Vesicular Basalts. J. Geol., 124, 435–445, https://doi.org/10.1086/686272, 2016.

Sandeep, S., Ajayamohan, R. S., Boos, W. R., Sabin, T. P., and Praveen, V.: Decline and poleward shift in Indian summer monsoon synoptic activity in a warming climate, P. Natl. Acad. Sci. USA., 115, 2681–2686, https://doi.org/10.1073/pnas.1709031115, 2018.

Środoń, J.: Mixed-layer illite-smectite in low-temperature diagenesis: data from the Miocene of the Carpathian Foredeep, Clay Miner., 19, 205–215, https://doi.org/10.1180/claymin.1984.019.2.07, 1984.

Sun, J. and Windley, B. F.: Onset of aridification by 34 Ma across the Eocene-Oligocene transition in Central Asia, Geology, 11, 1015–1018, https://doi.org/10.1130/G37165.1, 2015.

Takeuchi, A., Hren, M. T., Smith, S. V., Chamberlain, C. P., and Larson, P. B.: Pedogenic carbonate carbon isotopic constraints on paleoprecipitation: Evolution of desert in the Pacific Northwest, USA, in response to topographic development of the Cascade Range, Chem. Geol., 277, 323–335, https://doi.org/10.1016/j.chemgeo.2010.08.015, 2010.

Teraoka, Y., Suzuki, M., Tungalag, F., Ichinnorov, N., and Sakamaki, Y.: Tectonic framework of the Bayankhongor area, west Mongolia, Bulletin of the Geological Survey of Japan, 47, 447–455, 1996.

Wang, X., Carrapa, B., Sun, Y., Dettman, D. L., Chapman, J. B., Rugenstein, J. K. C., Clementz, M. T., DeCelles, P. G., Wang, M., Chen, J., Quade, J., Wang, F., Li, Z., Oimuhammadzoda, I., Gadoev, M., Lohmann, G., Zhang, X., and Chen, F.: The role of the westerlies and orography in Asian hydroclimate since the late Oligocene, Geology, 48, 728–732, https://doi.org/10.1130/G47400.1, 2020.

Wemmer, K., Steenken, A., Müller, S., de Luchi, M. G. L., and Siegesmund, S.: The tectonic significance of K/Ar illite fine-fraction ages from the San Luis formation (Eastern Sierras Pampeanas, Argentina), Int. J. Earth Sci., 100, 659–669, https://doi.org/10.1007/s00531-010-0629-8, 2011.

Winnick, M. J., Chamberlain, C. P., Caves, J. K., and Welker, J. M.: Quantifying the isotopic "continental effect", Earth Planet. Sci. Lett., 406, 123–133, https://doi.org/10.1016/j.epsl.2014.09.005, 2014.

Xiao, G. Q., Abels, H. A., Yao, Z. Q., Dupont-Nivet, G., and Hilgen, F. J.: Asian aridification linked to the first step of the Eocene-Oligocene climate Transition (EOT) in obliquity-dominated terrestrial records (Xining Basin, China), Clim. Past, 6, 501–513, https://doi.org/10.5194/cp-6-501-2010, 2010.

Zachos, J., Pagani, M., Sloan, L., Thomas, E., and Billups, K.: Trends, rhythms, and aberrations in global climate 65 Ma to present, Science, 292, 686–693, https://doi.org/10.1126/science.1059412, 2001.

Zamanian, K., Lechler, A. R., Schauer, A. J., Kuzyakov, Y., and Huntington, K. W.: The $\delta^{13}C$, $\delta^{18}O$ and Δ_{47} records in biogenic, pedogenic and geogenic carbonate types from paleosol-loess sequence and their paleoenvironmental meaning, Quat. Res., 101, 256–272, https://doi.org/10.1017/qua.2020.109, 2021.

Zhang, C., Wang, Y., Deng, T., Wang, X., Biasatti, D., Xu, Y., and Li, Q.: C4 expansion in the central Inner Mongolia during the latest Miocene and early Pliocene, Earth Planet. Sci. Lett., 287, 311–319, https://doi.org/10.1016/j.epsl.2009.08.025, 2009.

Zhang, Y. G., Pagani, M., Liu, Z., Bohaty, S. M., and Deconto, R.: A 40-million-year history of atmospheric CO_2, Philos. T. R. Soc. A, 371, 20130096, https://doi.org/10.1098/rsta.2013.0096, 2013.

Zorin, Y. A., Belichenko, V. G., Turutanov, E. K., Kozhevnikov, V. M., Ruzhentsev, S. V., Dergunov, A. B., Filippova, I. B., Tomurtogoo, O., Arvisbaatar, N., Bayasgalan, T., Biambaa, C., and Khosbayar, P.: The South Siberia-Central Mongolia transect, Tectonophysics, 225, 361–378, https://doi.org/10.1016/0040-1951(93)90305-4, 1993.